# ANNUAL VARIATION IN THE DEPTH OF 14°C IN THE TROPICAL PACIFIC OCEAN



A DISSERTATION SUBMITTED TO THE GRADUATE DIVISION OF THE UNIVERSITY OF HAWAII IN PARTIAL FULFILLMENT OF THE REQUIREMENTS FOR THE DEGREE OF

DOCTOR OF PHILOSOPHY

IN OCEANOGRAPHY

MAY 1978

By

Gary Meyers

Dissertation Committee:

Klaus Wyrtki, Chairman
Colin S. Ramage
Lorenz Magaard
Brent Gallagher
Edward D. Stroup

We certify that we have read this dissertation and that in our opinion it is satisfactory in scope and quality as a dissertation for the degree of Doctor of Philosophy in Oceanography.

DISSERTATION COMMITTEE

Klaus Wyrtki
Chairman

C. S. Ramage

Lorenz Magaard

Brent Gallagher

Edward D. Stroup

# ACKNOWLEDGMENTS

The author gratefully acknowledges the assistance of Shikiko Nakahara and Bernie Kilonsky who helped solve many of the programing problems that arise in analyzing large data sets on a computer.

# ABSTRACT

Annual variation in the depth of 14°C throughout the tropical Pacific Ocean between 30°N and 30°S is studied on the basis of 156,000 bathythermographs. Large amplitude variations are found in the region between 4°N and 15°N. Near 6°N the variations in depth propagate westward. Near 10°N they have the same phase across the ocean from the American coast to 145°E. A simple model of large-scale, low frequency currents can account for the variations. The model is driven by divergence in the Ekman layer set up by the surface wind stress, called Ekman pumping. It also incorporates the planetary, geostrophic divergence inherent on a rotating sphere. The rate of change in depth at 10°N is in phase with the Ekman pumping velocity. The geostrophic divergence is small because the variations do not have an appreciable east-west slope. Both Ekman pumping and geostrophic divergence are active at 6°N, because the oceanic response has the form of a westward propagating wave. This is a nearly resonant response due to the zonal length scale of the Ekman pumping velocity field, which is nearly equal to the half wave length of a free non-dispersive Rossby wave with a period of 1 year.

# TABLE OF CONTENTS

# LIST OF TABLES

# LIST OF ILLUSTRATIONS

# I. INTRODUCTION

The variation in strength and thermal structure of the Pacific Equatorial Currents in response to annual forcing by the trade winds is an example of air-sea interaction on the largest possible scale. The purpose of this study is to describe the variations in thermal structure and to relate them to the wind field. Observed vertical displacements of the thermocline are compared to displacements caused by two processes that dominate low-frequency oceanic circulation. The first is Ekman pumping, as defined by Veronis (1973). A variable wind stress acting on the sea surface with a frequency which is much smaller than the inertial frequency sets up a quasi-stationary Ekman layer; divergence of the Ekman transports yields a vertical velocity at the bottom of the Ekman layer. The thermocline is advected vertically by the Ekman pumping velocity if no other process that alters the thermal structure is active. Ekman pumping is illustrated in Fig. 1A, which shows easterly wind stress and northward Ekman transports in the northern hemisphere. The magnitude of the wind stress and of the transport is proportional to the length of the arrows. A region of divergence in the Ekman layer causes an upward velocity. The second process is the planetary, geostrophic divergence inherent on a rotating sphere (Stommel, 1957). It is illustrated in Fig. 1B. The sea surface slopes

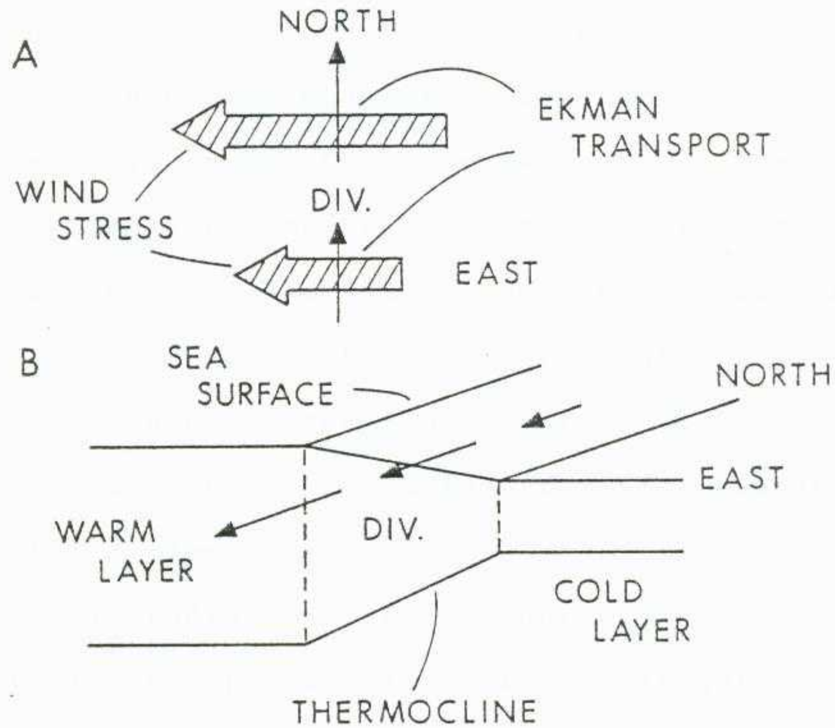


Fig. 1. Ekman pumping and geostrophic divergence.

upward to the west in a limited region, and is flat elsewhere. The slope is uniform in the north-south direction. The thermocline slopes in the opposite sense because the cold water in the lower layer is at rest. Arrows indicate a southward geostrophic current in the upper layer which increases in strength toward the equator due to decrease in the Coriolis parameter. The current is obviously divergent, and the thermocline is displaced upward in the absence of all forces other than the illustrated horizontal pressure gradient. This process will be called by the abbreviated name geostrophic divergence. The emergence of these processes from the equations of motion will be demonstrated in Chapter III.

Several studies carried out during the last decade have established the need for this investigation. Annual variation of the North Equatorial Current was first observed during the Trade Wind Zone Oceanography expedition (Seckel, 1968). A later study of the dynamic topography of the sea surface based on all the available oceanographic station data and on sea level observed at islands revealed that the North Equatorial Current and the Countercurrent are strongest from September to December and weakest from March to May, and that the South Equatorial Current is strongest when the two currents in the northern hemisphere are weakest (Wyrtki, 1974). Variation in the North Equatorial Current was related to the trade winds by

Meyers (1975), who found that vertical displacements of the thermocline in the Central Pacific are in phase with the Ekman pumping velocity calculated from the wind stress. White (1977) suggested that the agreement in phase occurs only near 150°W, but not at other longitudes, because a forced planetary wave propagates across the ocean between 10°N and 20°N. The monthly thermal structure in this region does not show the suggested wave (Robinson, 1976), but rather indicates that the North Equatorial Current reaches maximum strength at the same time at all longitudes. DeWitt and Leetma (1978) analyzed data from the Eastropac expedition and found that vertical displacements of the thermocline and the Ekman pumping velocity are in phase at 119°W. While there is no doubt that annual variations in the equatorial currents occur, their detailed description throughout the tropical Pacific is still lacking, and a consistent model showing how they are driven by the trade winds has not been achieved.

# II. DATA SOURCES AND DATA PROCESSING

## A. The depth of the 14°C isotherm

Low frequency variation in thermal structure is believed to be directly related to the variation in strength of geostrophic currents in the tropical Pacific Ocean (Meyers, 1974, 1975; Wyrtki *et al.*, 1977). Mapping of the thermal structure is the easiest method of observing variable currents because the measurement of temperature at depth is technologically simple compared to direct measurement of currents with moored current meters.

The methodology of a careful analysis of the climatological temperature-depth (T/Z) data is described in this chapter. The standard instruments used in gathering T/Z data are the mechanical bathythermograph (MBT), the expendable bathythermograph (XBT) and the hydrocast. Hydrocasts are somewhat redundant because an MBT or XBT is usually launched at each hydrocast station. In order to study climatological aspects of the thermal structure with the largest possible data set, all of the MBT and XBT data in the archives of the National Oceanographic Data Center (NODC), Washington, D. C. were acquired through R. Wert, NORPAX data manager. The MBT's were received on magnetic tape in August, 1974. The last update of this tape was in 1973. The XBT's were received in June 1976, and the last update was in 1975. Several tests were made to see if the tapes contained data from previous well known oceanographic cruises and the data archived at Fleet Numerical Weather Central, Monterey, Ca. While most of these tests were affirmative, some data from the Eastropic Expedition (King and Doty, 1957) and the Equapac Expedition (Austin, 1957) were missing. Wert (1976) has noted that 100,000 MBT slides held by NODC have not been processed due to lack of BT-logs and calibration data. It would be useful to see if the data from these expeditions are among the scrapped casts. Data in the region from 30°N to 30°S and 140°E to the American coast were sorted into 15 files, one for each 10° band of longitude, and the MBT's and XBT's were merged into a single data set. The merged data coverage is shown in Fig. 2. The areas north of the equator and near the North and South American coasts are the most densely sampled. Sampling in the South Pacific is best between 140°W and 170°W, but weak on either side of this zone.

Low frequency variability of the thermal structure in the tropical Pacific is characterized by vertical displacements of the thermocline which occur without change in the vertical temperature gradient. The correlation coefficient of the depth of 14°C vs. the depth of 18°C throughout the tropical Pacific is shown in Fig. 3. The coefficients were computed from all the T/Z casts within areas covering 2° of latitude and 10° of longitude. The coefficients are high throughout the tropical Pacific except near the

Fig. 2. Data coverage-bathythermographs. Number of casts per 5° square: black >1000, double hatched 500-1000, hatched 300-500, stippled 120-300, blank <120.

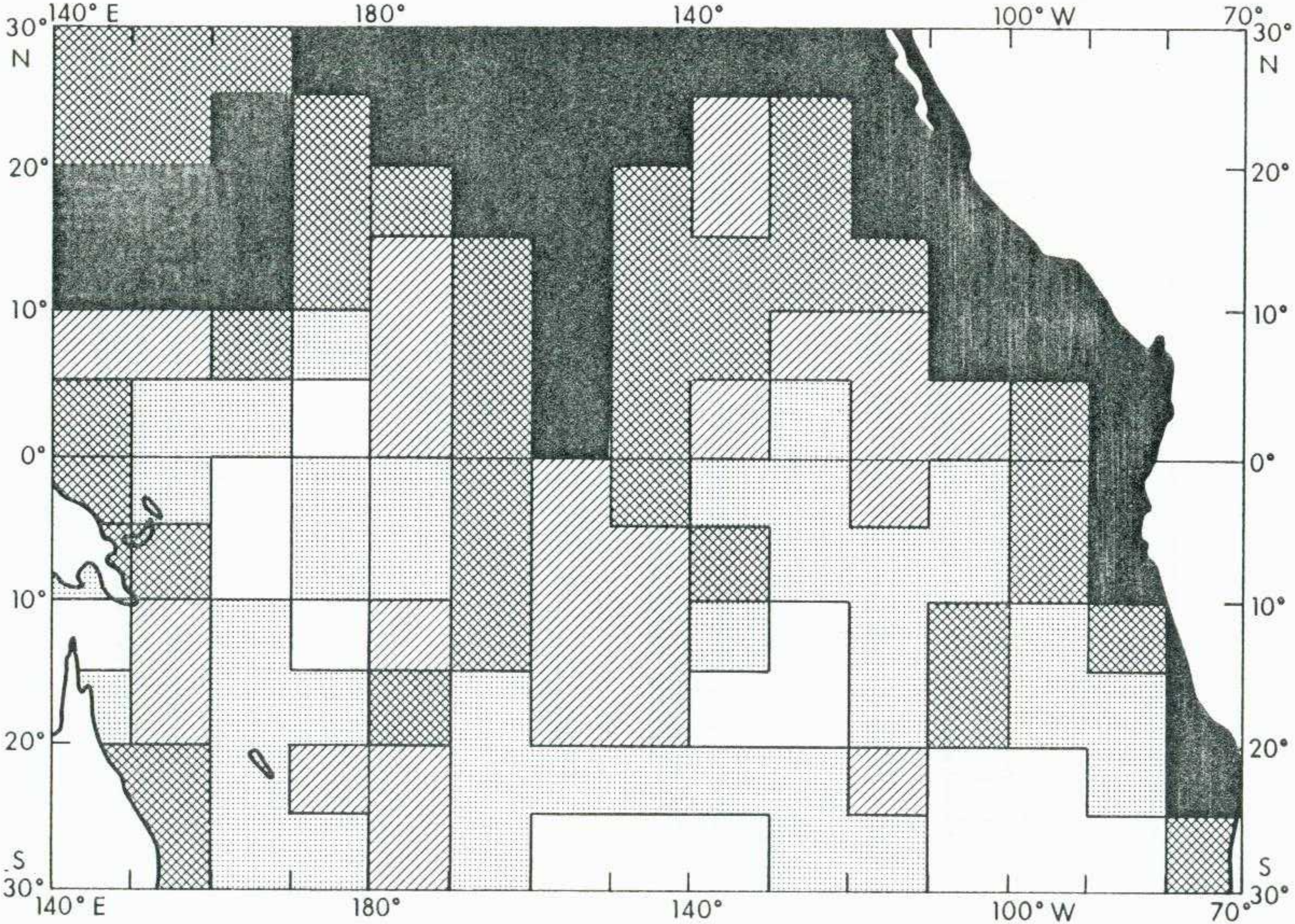


Fig. 2. See caption on facing page.

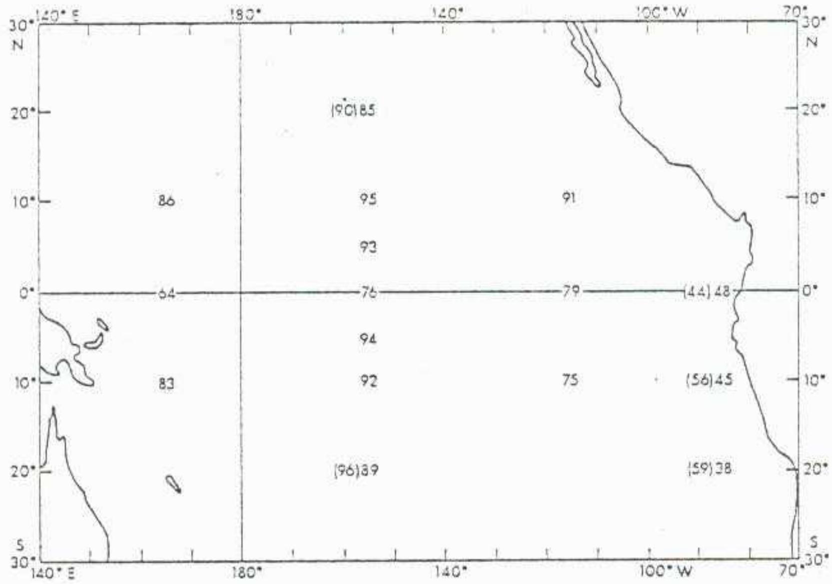


Fig. 3. Correlation coefficient of the depth of 14°C vs. depth of 18°C. (14°C vs. 11°C in parentheses).

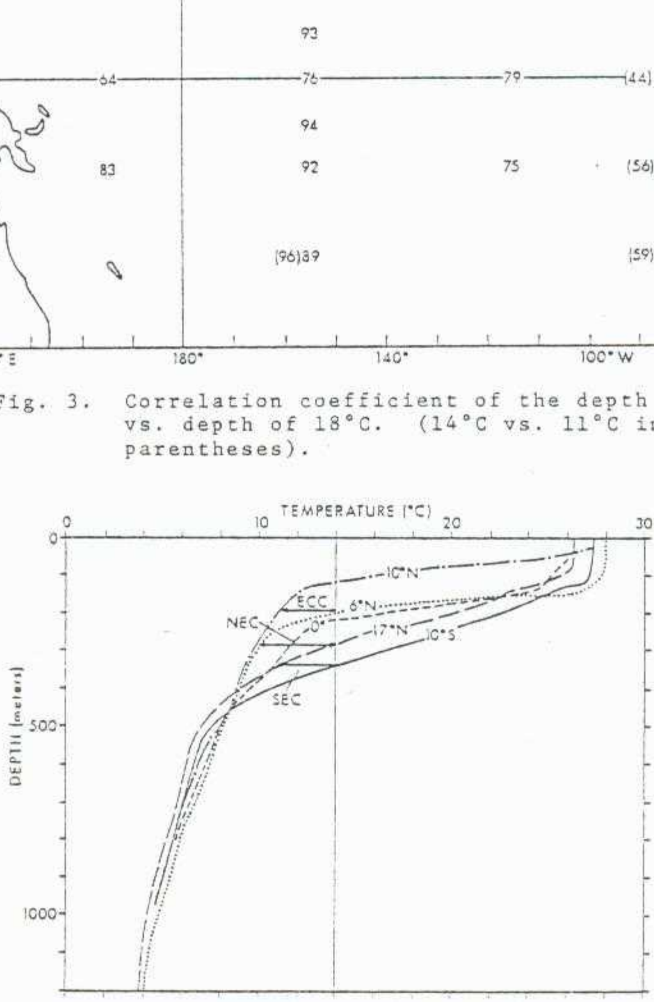


Fig. 4. Vertical temperature structure at 160°W observed during the Equapac expedition (Austin, 1957).

eastern boundary. They are slightly smaller along the equator as would be expected. They are also smaller toward the centers of the subtropical gyres. The correlation of the depth of 14°C with the depth of 11°C is shown in parentheses. The deeper isotherms are very highly correlated in the centers of the subtropical gyres. Apparently the depth of 14°C is more representative of the variability of subtropical gyres than the depth of 18°C because the shallower isotherm is influenced by surface heat exchange at higher latitudes (Wyrtki et. al., 1977). A nearly complete description of the variability of the thermal structure can be achieved by mapping the topography of one isotherm in the tropical Pacific because the vertical temperature gradient is nearly constant in time.

Several criteria influence the selection of an isotherm. It should be deep enough so that it is not affected by heat exchange through the surface. This requires that it be deeper than the maximum vertical density gradient, whose stability suppresses mixing. It should also be deeper than the bottom of the near surface layer in rapid baroclinic motion. However it cannot be so deep that the vertical temperature gradient is small, because the error in calculating the depth of an isotherm is large in this case. The depth of 14°C ($D_{14}$) satisfies these criteria as seen in Fig. 4. It is clearly below the most rapid portions of the North Equatorial Current (NEC), the South Equatorial Current (SEC) and the Countercurrent (ECC), and above the level of weak vertical gradients. It should be noted that a majority of T/Z casts in the western Pacific do not reach the depth of 14°C; consequently, the data coverage for this isotherm is not as good as shown in Fig. 2. The temperature structure of the upper 150 m in the western Pacific has been thoroughly analyzed by Robinson (1976) and White and Wylie (1977). Therefore the shallower isotherms were not analyzed in this study.

The use of MBT's and XBT's imposes limits on the accuracy of the data. Vertical temperature gradients are accurately measured by MBT's but the in situ temperature is not. Overall system errors including digitizing range from ±.2°C to ±1.5°C (Wert, 1976). The approximate error in calculating the depth of 14°C is the quotient of a typical error in temperature measurement, say 1°C, and a typical vertical temperature gradient, .12°C/m, which equals 8 m. The temperature measured by XBT is considerably more accurate, ranging from ±.03 to ±.2°C; however, the error in measured depth is about 5 m (Wert, 1976). The system used in gathering T/Z data for this study does not permit resolution of the annual signal where the amplitude is less than approximately 8 m.

The merged data set was analyzed by two independent procedures. The data were first very carefully analyzed by hand. This procedure involved many subjective decisions, as does any hand analysis. It is essential to gain confidence that the main features of the analyzed field are independent of the subjective decisions. Therefore the data were analyzed a second time by a completely objective technique which is described later. The two analyses were compared, and only features which appeared in both were studied further.

The hand analysis was carried out as follows. First $D_{14}$ was averaged in 1°-squares where the number of observations exceeded 4 during a month, and the mean value, standard deviation and number of casts was stored. Meridional sections of $D_{14}$ in the form of scatter diagrams were then plotted for each 10° of longitude (Fig. 5), and a smooth contour was drawn through the points by hand. Where the sampling density was weak, the contour was drawn with the aid of data from the preceeding or following month or from an adjacent longitude. The contour was digitized at each 2° of latitude and stored on cards. Fourier coefficients were computed from the 12 monthly values at each grid point. The statistical significance of the 2nd and higher harmonics was tested using the F-ratio (Hayes, 1970, p. 51), and those harmonics which did not pass at the 10% level were set equal to zero. Very few higher harmonics passed except near the eastern boundary. $D_{14}$ was calculated again from the significant harmonic coefficients. Then spatial fluctuations with a zonal scale of 20° of longitude were

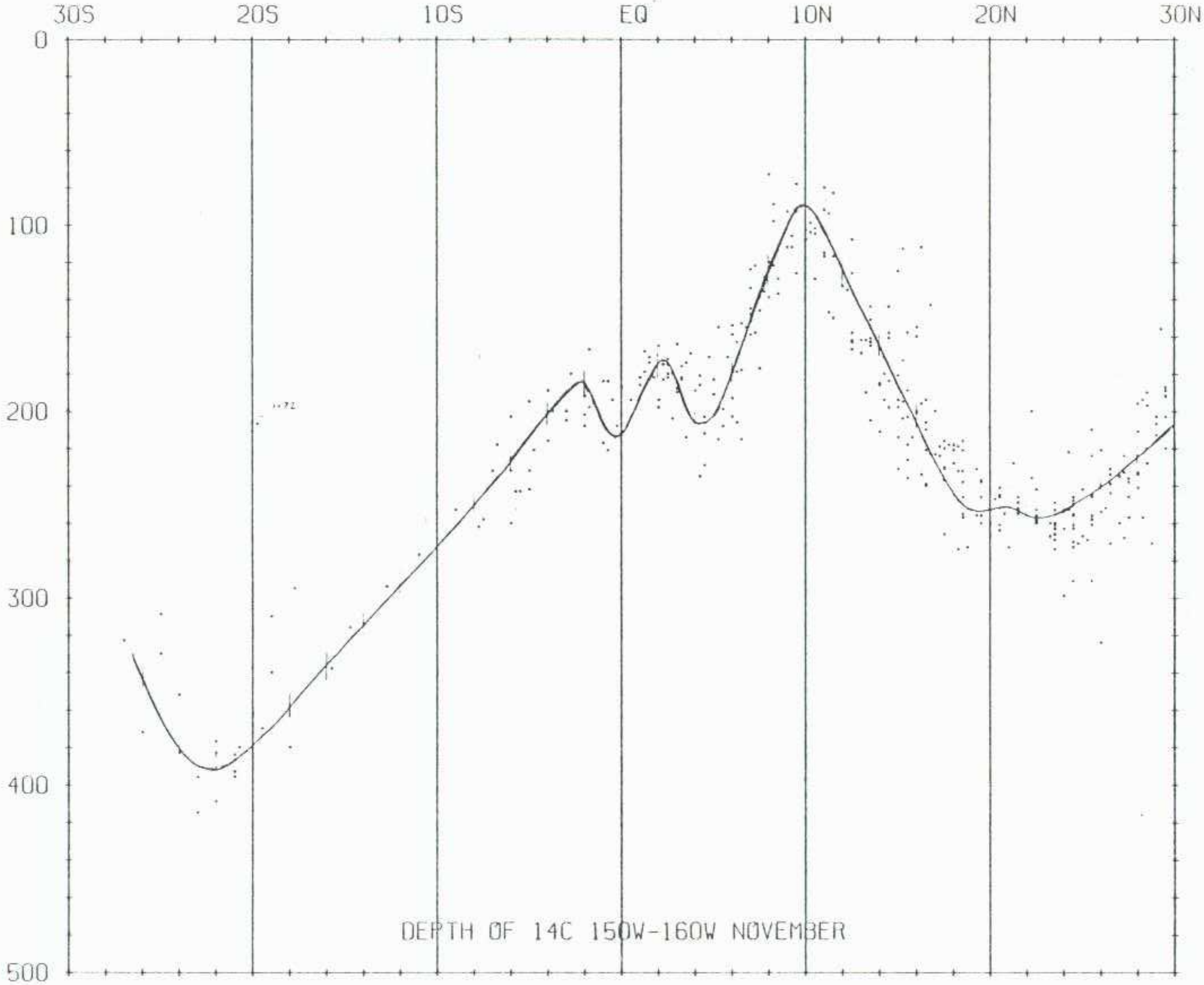


Fig. 5. Depth of 14°C near 155°W in November.

removed by filtering with a ¼, ½, ¼ weighted zonal running mean.

In order to analyze the data objectively, all of the casts in a large region were represented by a function (D) of latitude ($\theta$), longitude ($\lambda$) and time (t)

$$D = M(\theta,\lambda) + C(\theta,\lambda) \cos \omega t + S(\theta,\lambda) \sin \omega t$$

$$\omega = 2\pi/12$$

$$M(\theta,\lambda) = \sum_{i=1}^{10} m_i F_i$$

$$C(\theta,\lambda) = \sum_{i=1}^{10} c_i F_i$$

$$S(\theta,\lambda) = \sum_{i=1}^{10} s_i F_i$$

$$F_1 = 1 \qquad F_2 = \theta \qquad F_3 = \lambda$$

$$F_4 = \theta^2 \qquad F_5 = \theta\lambda \qquad F_6 = \lambda^2$$

$$F_7 = \theta^3 \qquad F_8 = \theta^2\lambda \qquad F_9 = \theta\lambda^2$$

$$F_{10} = \lambda^3$$

The $m_i$, $c_i$ and $s_i$, i = 1, 2, ... 10 were determined by the method of least squares. The amplitude $(S^2 + C^2)^{\frac{1}{2}}$ for areas of different size are shown in Fig. 6A.

The number of observations used in each calculation and the RMS error of estimate ($\sigma$) is also shown. The error of estimate increases as the area extends further northward because the amplitude of the annual signal decreases toward the north. Variance about the mean topography ($\sigma_m$) can also be calculated and an interesting statistic is the percent reduction in variance (R) by the sinusoidal terms

$$R = 100 \times \frac{(\sigma_m - \sigma)}{\sigma_m}$$

The statistic R decreases as the area extends further northward, but is not changed if the area covers a wider range of longitude. The influence of the spatial variability of sampling density is seen in Fig. 6A by comparing the panels for 6°N-10°N, 160°W-180°W and 6°N-10°N, 140°W-180°W. The first was calculated from 729 observations; it shows an amplitude of less than 10 m near 12°N, 175°W. The adjacent 6° x 20° rectangle is more densely sampled, consequently the second panel was calculated from 2723 observations. The larger annual amplitude in the densely sampled area has been imposed on the region near 12°N, 175°W. Details of the objective analysis as well as estimated statistics like $\sigma$ and R are dependent on the extent of the region. Use of a region of uniform size throughout the area under study seemed desirable. Therefore the regions were limited to 20° of longitude

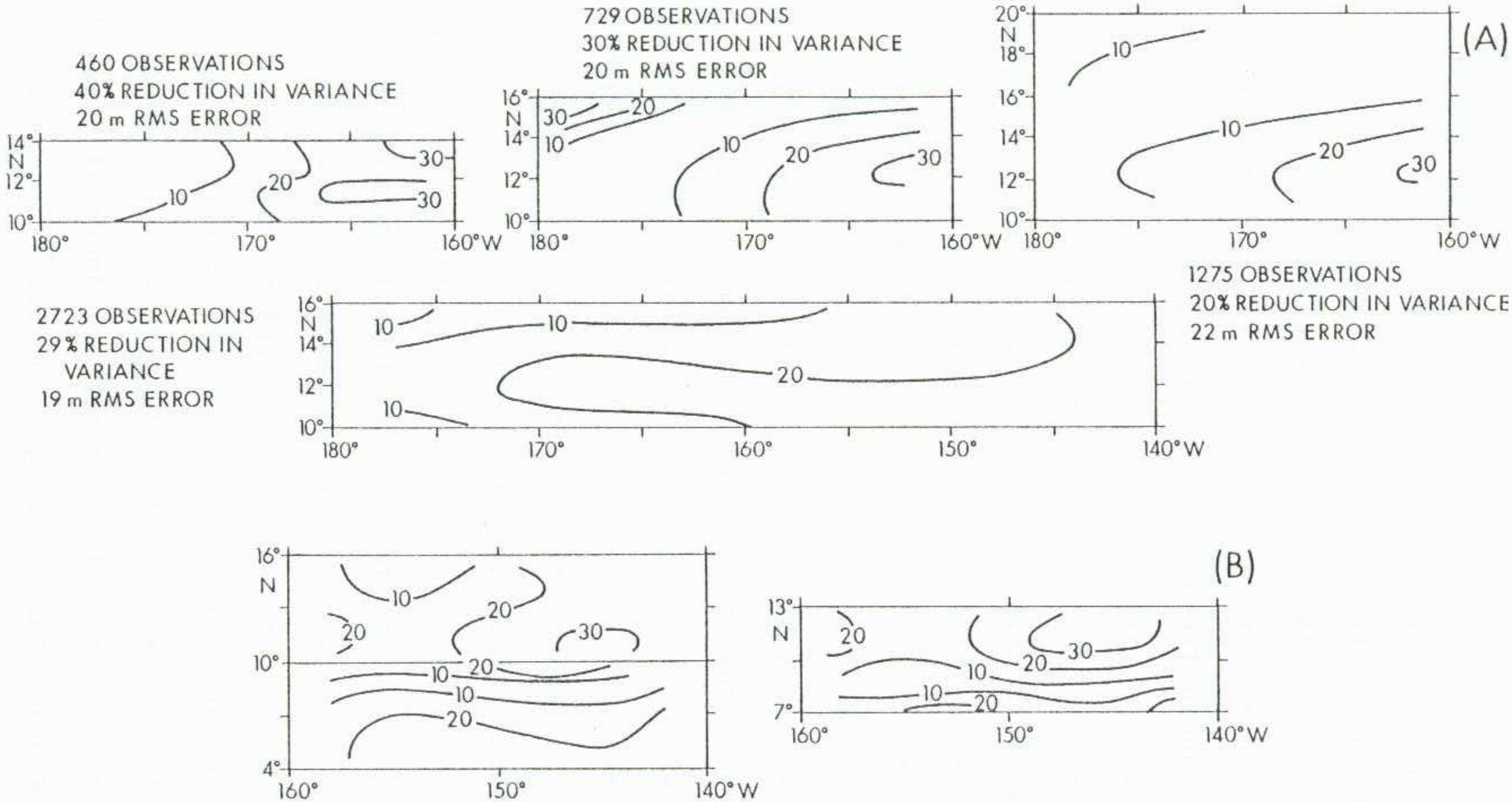


Fig. 6. Amplitude of the sinusoidal terms.

in order to reduce the effect of spatially variable sampling density. Larger regions would combine poorly sampled areas with well sampled areas (Fig. 2). The latitudinal extent is limited by the use of cubic polynomials. A ridge in the amplitude of the annual signal can probably be well represented by the polynomials but not two adjacent ridges. The regions were limited to 6° of latitude because the hand analysis had already revealed that ridges would occur near 5°N and 11°N. The stability of solutions for areas covering 6° of latitude and 20° of longitude can be demonstrated by calculating the amplitude in overlapping areas (Fig. 6B). Although the three panels are calculated from different data, the three representations are highly consistent. Stability is dependent on the density of the observations. Instability was found in areas where the number of observations was less than 200. The determinant of the matrix of coefficients of the 30 unknown $m_i$, $c_i$, and $s_i$'s, usually had a value less than 1 in this case. The RMS error of estimate ($\sigma$) throughout the region being studied is shown in Fig. 7. It is between 15 and 20 m except near the eastern boundary and in the area south of Japan. The error is due to fluctuations at all frequencies other than 1 cycle per year and is the "noise" in which the annual variations are embedded. The percent reduction in variance about the mean (R) achieved by the annual sinusoidal terms is shown in Fig. 8.

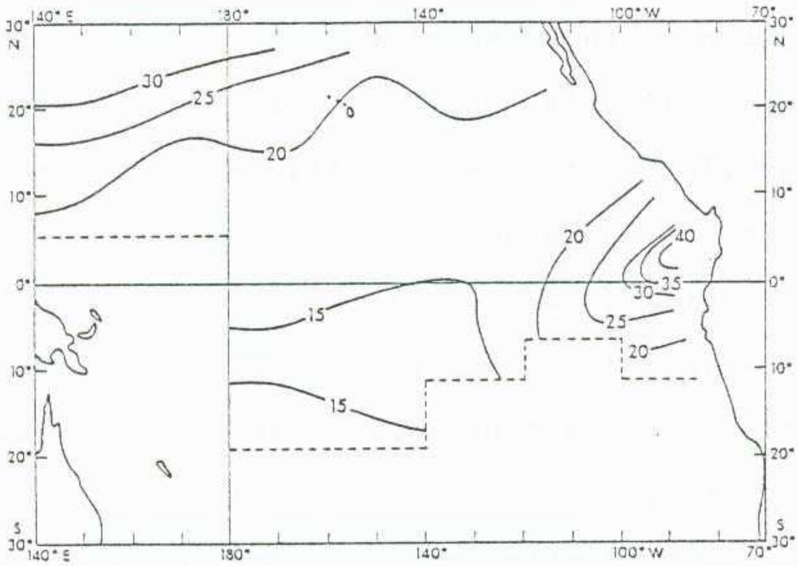


Fig. 7. Standard error of estimate.

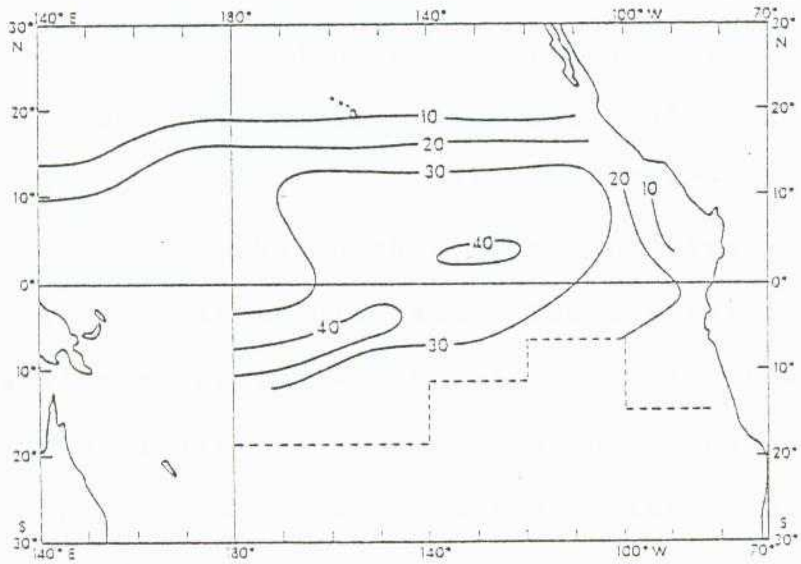


Fig. 8. Percent reduction in variance.

The reduction exceeds 30% over a wide area in the tropical Pacific. The objectively analyzed anomalies were also filtered with a ¼, ½, ¼ weighted zonal running mean.

Comparison of the hand and objective analyses for November tests the reliability of the analyzed data (Figs. 9 and 10). The areas where the magnitude of the anomaly in $D_{14}$ exceeds 10 m is enclosed by lines. The two analyses are in remarkably good agreement in the areas of large displacements. It should be noted that in the South Pacific near 10°S, 110°W the hand analysis (Fig. 10) shows large anomalies which emerged essentially from data taken during the Eastropac cruises in 1967 and 1968 (Love, 1971, 1972a, 1972b, 1973, 1975). This anomaly did not appear in the earlier data analyzed by Wyrtki (1964). It is at this time not clear whether the anomalies near 10°S, 110°W are due to annual or interannual fluctuations. The reliability of the analyzed data can be further tested by direct comparison to the original scatter diagrams. The scatter diagram and hand analysis for 150°W-160°W in April is shown in Fig. 11. The hand analysis for November (dashed line) is superimposed on the April data. The deviations between the November analysis and the April data leave little doubt that the anomalies between the equator and 15°N in the Central Pacific are real features of the circulation.

The hand analysis is used for the remainder of this study because I have greater confidence in it. Where data

| NOV | 145E | 155E | 165E | 175E | 175W | 165W | 155W | 145W | 135W | 125W | 115W | 105W | 95W | 85W | 75W |
|---|---|---|---|---|---|---|---|---|---|---|---|---|---|---|---|
| 30N | 9999. | 9999. | 9999. | 9999. | 9999. | 9999. | 9999. | 9999. | 9999. | 9999. | 9999. | 9999. | 9999. | 9999. | 9999. |
| 28N | 11. | 5. | 3. | 6. | 7. | 4. | 1. | 2. | 4. | 5. | 9999. | 9999. | 9999. | 9999. | 9999. |
| 26N | 5. | 0. | 0. | 1. | -2. | -4. | -1. | 4. | 6. | 5. | 9999. | 9999. | 9999. | 9999. | 9999. |
| 24N | -0. | 2. | 5. | 3. | 1. | 1. | -0. | -1. | -0. | -2. | 9999. | 9999. | 9999. | 9999. | 9999. |
| 22N | 0. | 3. | -0. | -3. | -1. | 1. | -1. | -2. | 2. | 6. | 12. | 23. | 9999. | 9999. | 9999. |
| 20N | 9. | 2. | -2. | -2. | -1. | 1. | -0. | -1. | 2. | 4. | 1. | -8. | 9999. | 9999. | 9999. |
| 18N | 9. | 3. | -3. | -6. | -7. | -3. | 1. | 3. | 3. | 5. | 1. | -8. | 9999. | 9999. | 9999. |
| 16N | 7. | 7. | 1. | -4. | 0. | 5. | 8. | 10. | 8. | 7. | 6. | -2. | 9999. | 9999. | 9999. |
| 14N | 8. | 7. | 7. | 4. | 6. | 11. | 14. | 17. | 17. | 14. | 14. | 11. | 9999. | 9999. | 9999. |
| 12N | 12. | 5. | 9. | 8. | 11. | 17. | 21. | 23. | 17. | 13. | 15. | 18. | 9999. | 9999. | 9999. |
| 10N | 11. | 6. | 10. | 12. | 15. | 18. | 20. | 18. | 10. | 8. | 13. | 20. | 9999. | 9999. | 9999. |
| 08N | 4. | 5. | 7. | 8. | 7. | 1. | -7. | -7. | -10. | -16. | -9. | 5. | 7. | -8. | 9999. |
| 06N | 9999. | 9999. | 9999. | 9999. | -12. | -18. | -21. | -16. | -14. | -20. | -18. | -4. | 3. | -8. | 9999. |
| 04N | 9999. | 9999. | 9999. | 9999. | -14. | -15. | -20. | -24. | -21. | -15. | -15. | -6. | -0. | -6. | 9999. |
| 02N | 9999. | 9999. | 9999. | 9999. | -5. | -9. | -11. | -15. | -14. | -12. | -12. | -6. | 3. | 10. | 9999. |
| EQ | 9999. | 9999. | 9999. | 9999. | -8. | -7. | -4. | -7. | -9. | -5. | 6. | 12. | 15. | 44. | 9999. |
| 02S | 9999. | 9999. | 9999. | 9999. | -7. | -8. | -9. | -14. | -16. | -11. | -7. | -4. | 11. | 38. | 9999. |
| 04S | 9999. | 9999. | 9999. | 9999. | -11. | -4. | -12. | -16. | -14. | -14. | -13. | -11. | -0. | 17. | 9999. |
| 06S | 9999. | 9999. | 9999. | 9999. | -26. | -6. | -4. | -6. | -7. | -21. | 9999. | 9999. | -9. | 2. | 9999. |
| 08S | 9999. | 9999. | 9999. | 9999. | -0. | 16. | 10. | 0. | -4. | -13. | 9999. | 9999. | -5. | 0. | 9999. |
| 10S | 9999. | 9999. | 9999. | 9999. | 11. | 10. | 7. | -1. | 9999. | 9999. | 9999. | 9999. | -9. | -6. | 9999. |
| 12S | 9999. | 9999. | 9999. | 9999. | 9. | 9. | 8. | 3. | 9999. | 9999. | 9999. | 9999. | -23. | -10. | 9999. |
| 14S | 9999. | 9999. | 9999. | 9999. | -4. | -1. | -4. | -9. | 9999. | 9999. | 9999. | 9999. | -22. | -15. | 9999. |
| 16S | 9999. | 9999. | 9999. | 9999. | 3. | 4. | 3. | -6. | 9999. | 9999. | 9999. | 9999. | 9999. | 9999. | 9999. |
| 18S | 9999. | 9999. | 9999. | 9999. | 1. | 7. | 8. | 7. | 9999. | 9999. | 9999. | 9999. | 9999. | 9999. | 9999. |
| 20S | 9999. | 9999. | 9999. | 9999. | 9999. | 9999. | 9999. | 9999. | 9999. | 9999. | 9999. | 9999. | 9999. | 9999. | 9999. |
| 22S | 9999. | 9999. | 9999. | 9999. | 9999. | 9999. | 9999. | 9999. | 9999. | 9999. | 9999. | 9999. | 9999. | 9999. | 9999. |
| 24S | 9999. | 9999. | 9999. | 9999. | 9999. | 9999. | 9999. | 9999. | 9999. | 9999. | 9999. | 9999. | 9999. | 9999. | 9999. |
| 26S | 9999. | 9999. | 9999. | 9999. | 9999. | 9999. | 9999. | 9999. | 9999. | 9999. | 9999. | 9999. | 9999. | 9999. | 9999. |
| 28S | 9999. | 9999. | 9999. | 9999. | 9999. | 9999. | 9999. | 9999. | 9999. | 9999. | 9999. | 9999. | 9999. | 9999. | 9999. |
| 30S | 9999. | 9999. | 9999. | 9999. | 9999. | 9999. | 9999. | 9999. | 9999. | 9999. | 9999. | 9999. | 9999. | 9999. | 9999. |

Fig. 9. Objective analysis - November.

| NOV | 145E | 155E | 165E | 175E | 175W | 165W | 155W | 145W | 135W | 125W | 115W | 105W | 95W | 85W | |
|---|---|---|---|---|---|---|---|---|---|---|---|---|---|---|---|
| 30N | 11. | 7. | 1. | -3. | 9999. | 9999. | -7. | 8. | 4. | 9999. | 9999. | 9999. | 9999. | 9999. | 9999. |
| 28N | 10. | 6. | 3. | 3. | 3. | 0. | -2. | 2. | 3. | 0. | -4. | 9999. | 9999. | 9999. | 9999. |
| 26N | 8. | 5. | 4. | 5. | 2. | -2. | -2. | 0. | 1. | -2. | -4. | 9999. | 9999. | 9999. | 9999. |
| 24N | 7. | 4. | 3. | 3. | -1. | -3. | -3. | -2. | -2. | -4. | -4. | 9999. | 9999. | 9999. | 9999. |
| 22N | 7. | 4. | 1. | -3. | -3. | 1. | 0. | -1. | -3. | -4. | -4. | -5. | 9999. | 9999. | 9999. |
| 20N | 6. | 4. | 1. | -4. | -2. | 3. | 3. | 1. | 0. | -2. | -2. | -3. | 9999. | 9999. | 9999. |
| 18N | 5. | 5. | 2. | -3. | -2. | -1. | 0. | 3. | 4. | 3. | 2. | -4. | 9999. | 9999. | 9999. |
| 16N | 4. | 9. | 6. | 2. | 3. | 4. | 7. | 12. | 10. | 8. | 7. | -1. | 9999. | 9999. | 9999. |
| 14N | 7. | 10. | 9. | 6. | 7. | 11. | 13. | 14. | 15. | 16. | 15. | 8. | -4. | 9999. | 9999. |
| 12N | 10. | 13. | 11. | 8. | 11. | 19. | 22. | 20. | 16. | 18. | 18. | 15. | 5. | 9999. | 9999. |
| 10N | 4. | 9. | 13. | 17. | 12. | 16. | 19. | 17. | 12. | 10. | 15. | 14. | 10. | -1. | -1. |
| 08N | 6. | 3. | 0. | 1. | 2. | 2. | -1. | -5. | -8. | -10. | -4. | 5. | 5. | 1. | 4. |
| 06N | 4. | -5. | -14. | -12. | -14. | -18. | -21. | -19. | -15. | -19. | -16. | -2. | 7. | 6. | 6. |
| 04N | 9. | 8. | 0. | -8. | -13. | -13. | -11. | -14. | -17. | -16. | -9. | 0. | 8. | 9. | 7. |
| 02N | 8. | 6. | -3. | -14. | -15. | -12. | -14. | -17. | -12. | -6. | -4. | 0. | 9. | 15. | 15. |
| EQ | 5. | 3. | -3. | -12. | -9. | -4. | -7. | -9. | -5. | 2. | 9. | 12. | 13. | 17. | 15. |
| 02S | 9999. | 9999. | 9999. | 9999. | -9. | -9. | -10. | -11. | -7. | -4. | -2. | 2. | 5. | 7. | 6. |
| 04S | 9999. | 9999. | 9999. | 9999. | -8. | -9. | -11. | -13. | -10. | -10. | -10. | -8. | 0. | 7. | 7. |
| 06S | 9999. | 9999. | 9999. | 9999. | -4. | -5. | -6. | -5. | -4. | -9. | -14. | -12. | -6. | -1. | 1. |
| 08S | 9999. | 9999. | 9999. | 9999. | -4. | -1. | 0. | 0. | -2. | -9. | -13. | -11. | -9. | -2. | 9999. |
| 10S | 9999. | 9999. | 9999. | 9999. | -3. | 2. | 2. | 0. | -1. | -6. | -11. | -13. | -12. | -2. | 6. |
| 12S | 9999. | 9999. | 9999. | 9999. | 0. | 3. | 2. | -1. | -2. | -5. | -10. | -10. | -6. | 1. | 6. |
| 14S | 9999. | 9999. | 9999. | 9999. | 0. | 2. | 2. | 2. | 1. | -1. | -5. | -7. | -5. | -2. | 0. |
| 16S | 9999. | 9999. | 9999. | 9999. | -1. | 0. | -1. | -1. | 0. | 1. | -3. | -7. | -7. | -5. | -4. |
| 18S | 9999. | 9999. | 9999. | 9999. | -2. | -1. | -1. | -1. | 2. | 9999. | 9999. | 9999. | 9999. | 3. | -5. |
| 20S | 9999. | 9999. | 9999. | 9999. | 9999. | 9999. | 9999. | 9999. | 9999. | 9999. | 9999. | 9999. | 9999. | 9999. | 9999. |
| 22S | 9999. | 9999. | 9999. | 9999. | 9999. | 9999. | 9999. | 9999. | 9999. | 9999. | 9999. | 9999. | 9999. | 9999. | 9999. |
| 24S | 9999. | 9999. | 9999. | 9999. | 9999. | 9999. | 9999. | 9999. | 9999. | 9999. | 9999. | 9999. | 9999. | 9999. | 9999. |
| 26S | 9999. | 9999. | 9999. | 9999. | 9999. | 9999. | 9999. | 9999. | 9999. | 9999. | 9999. | 9999. | 9999. | 9999. | 9999. |
| 28S | 9999. | 9999. | 9999. | 9999. | 9999. | 9999. | 9999. | 9999. | 9999. | 9999. | 9999. | 9999. | 9999. | 9999. | 9999. |
| 30S | 9999. | 9999. | 9999. | 9999. | 9999. | 9999. | 9999. | 9999. | 9999. | 9999. | 9999. | 9999. | 9999. | 9999. | 9999. |

Fig. 10. Hand analysis - November.

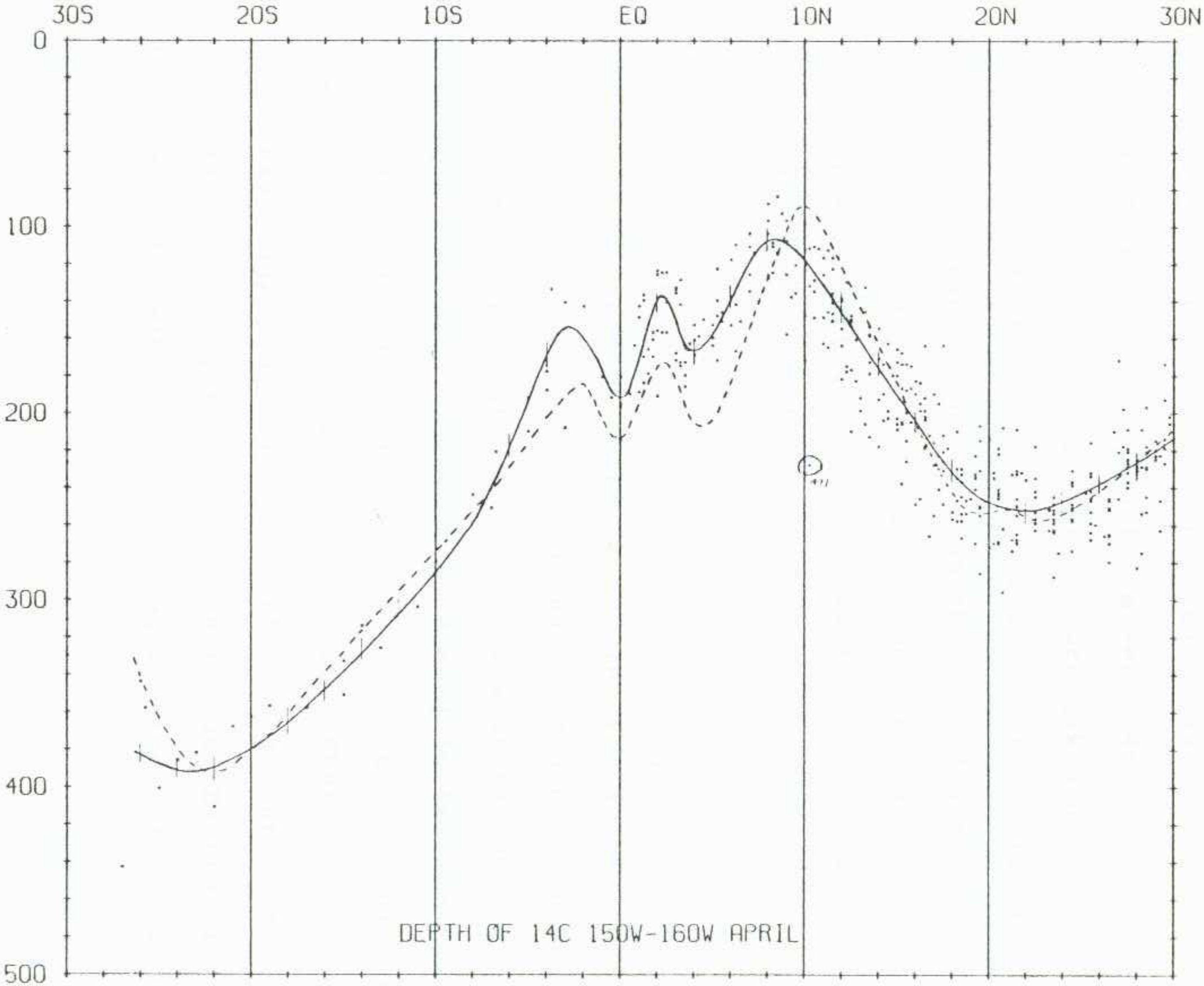


Fig. 11. Depth of 14°C near 155°W in April.

are sparse, the hand analysis is at least always representative of the few data that exist in the region. Very anomalous observations which deviated from the analyzed values by more than 100 m were easily identified and eliminated. Highly anomalous data taken during 1971 and 1972 are circled in Figs. 5 and 11. The objective analysis is dominated by the densely sampled areas, and its quality control is not as simple. Only those features which appeared in both the hand and the objective analyses are discussed in detail.

B. The wind field

Annual variation in the trade wind field over the Pacific Ocean was studied on the basis of 5 million wind observations made by ships. The data sources and data processing have been discussed in detail in two technical reports (Wyrtki and Meyers, 1975 a, b). In particular the calculation of the differential operator CURL was described. The annual variation of the wind field has been discussed in detail in a separate article (Wyrtki and Meyers, 1976). The spatial distribution of wind observations is shown in Fig. 12.

| | 125E | 135E | 145E | 155E | 165E | 175E | 175W | 165W | 155W | 145W | 135W | 125W | 115W | 105W | 95W | 85W | 75W |
|---|---|---|---|---|---|---|---|---|---|---|---|---|---|---|---|---|---|
| 29N | 54045 | 66954 | 20351 | 23291 | 25410 | 26510 | 32552 | 17371 | 13496 | 53252 | 33582 | 11570 | 38116 | 0 | 0 | 0 | 0 |
| 27N | 90802 | 51362 | 17446 | 13747 | 20746 | 20729 | 20370 | 16487 | 13027 | 59381 | 10857 | 10803 | 47886 | 0 | 0 | 0 | 0 |
| 25N | 72044 | 39826 | 20677 | 14262 | 13392 | 15078 | 20648 | 19417 | 27180 | 26734 | 6430 | 8442 | 54006 | 0 | 0 | 0 | 0 |
| 23N | 69594 | 34815 | 20426 | 10428 | 9060 | 11763 | 18793 | 38738 | 38671 | 8010 | 5812 | 6086 | 46695 | 0 | 0 | 0 | 0 |
| 21N | 57118 | 27681 | 18676 | 12123 | 12075 | 13894 | 20489 | 39648 | 47444 | 22242 | 17609 | 6253 | 8958 | 0 | 0 | 0 | 0 |
| 19N | 64654 | 21714 | 22247 | 12358 | 13637 | 13056 | 10243 | 17307 | 15542 | 8182 | 13152 | 20566 | 6792 | 65805 | 0 | 0 | 0 |
| 17N | 31666 | 20848 | 22348 | 15069 | 7516 | 4246 | 7279 | 8980 | 6013 | 5575 | 7220 | 10190 | 4300 | 64955 | 19422 | 0 | 0 |
| 15N | 51799 | 17975 | 33669 | 8781 | 2942 | 5620 | 5522 | 5516 | 3181 | 3641 | 4174 | 5534 | 11838 | 19206 | 80428 | 0 | 0 |
| 13N | 45474 | 18959 | 25700 | 10482 | 7521 | 5605 | 2530 | 4911 | 2724 | 2984 | 3316 | 3494 | 6372 | 17836 | 73619 | 0 | 0 |
| 11N | 28689 | 6921 | 16403 | 7491 | 15841 | 6014 | 1422 | 4869 | 2891 | 2622 | 3011 | 2053 | 2647 | 7423 | 39489 | 0 | 0 |
| 9N | 0 | 7327 | 6576 | 4236 | 7399 | 3077 | 1223 | 4492 | 2320 | 2109 | 2741 | 1948 | 2136 | 2643 | 15655 | 85612 | 19336 |
| 7N | 9793 | 7268 | 6902 | 7405 | 3745 | 3199 | 1603 | 4760 | 2936 | 2778 | 3156 | 2965 | 2942 | 2695 | 5508 | 65896 | 13014 |
| 5N | 8681 | 3492 | 4234 | 2098 | 4342 | 1173 | 1579 | 4181 | 2808 | 1670 | 1789 | 1703 | 1495 | 935 | 3162 | 23174 | 3977 |
| 3N | 9155 | 2336 | 4256 | 2680 | 1023 | 1200 | 1510 | 3829 | 2685 | 1656 | 1243 | 1486 | 1389 | 1150 | 7856 | 19443 | 3931 |
| 1N | 5465 | 1616 | 3341 | 3803 | 846 | 1151 | 1957 | 7466 | 1841 | 1628 | 996 | 1272 | 1451 | 3216 | 8966 | 17656 | 1587 |
| 1S | 0 | 0 | 4449 | 4595 | 1538 | 996 | 2490 | 2588 | 1686 | 1534 | 841 | 2691 | 2948 | 6533 | 7320 | 17695 | 0 |
| 3S | 0 | 0 | 5535 | 5795 | 1312 | 1061 | 3071 | 2573 | 1812 | 1568 | 776 | 2565 | 5402 | 6141 | 10247 | 15019 | 0 |
| 5S | 0 | 0 | 2317 | 6155 | 1340 | 1012 | 2533 | 2721 | 1543 | 1482 | 982 | 3565 | 6018 | 5484 | 10593 | 9071 | 0 |
| 7S | 0 | 0 | 0 | 8814 | 1543 | 1150 | 2702 | 2788 | 1512 | 1635 | 1343 | 6385 | 3952 | 4960 | 10689 | 8405 | 914 |
| 9S | 0 | 0 | 0 | 11044 | 4767 | 2664 | 2745 | 2694 | 1837 | 1814 | 4113 | 4815 | 3977 | 7214 | 6834 | 3757 | 5841 |
| 11S | 3346 | 11322 | 16564 | 10959 | 4574 | 1321 | 2998 | 2761 | 1735 | 3483 | 4934 | 2021 | 3809 | 8820 | 3113 | 1830 | 6622 |
| 13S | 1989 | 2746 | 6695 | 7740 | 4595 | 1589 | 4268 | 2608 | 2502 | 5291 | 2741 | 2917 | 3284 | 9160 | 1888 | 1171 | 7322 |
| 15S | 2030 | 0 | 11190 | 7180 | 5501 | 2808 | 7264 | 4305 | 3757 | 3742 | 1377 | 3788 | 5551 | 6365 | 1265 | 686 | 8246 |
| 17S | 1928 | 0 | 8809 | 6156 | 8857 | 4714 | 4533 | 3283 | 5594 | 2282 | 2716 | 2906 | 7650 | 4013 | 1157 | 651 | 9185 |
| 19S | 607 | 0 | 8041 | 5500 | 5297 | 7313 | 3557 | 3673 | 4551 | 758 | 4007 | 3161 | 7790 | 2809 | 941 | 756 | 7447 |
| 21S | 0 | 0 | 400 | 4708 | 3759 | 6125 | 4374 | 2630 | 3137 | 2344 | 2648 | 6869 | 4648 | 1651 | 858 | 1023 | 9181 |
| 23S | 0 | 0 | 0 | 7382 | 9149 | 7086 | 2619 | 3476 | 1738 | 3252 | 2163 | 8298 | 3506 | 837 | 682 | 1286 | 9132 |
| 25S | 0 | 0 | 0 | 6869 | 7929 | 5209 | 2762 | 3734 | 3088 | 2108 | 6299 | 6570 | 2922 | 535 | 572 | 1995 | 8185 |
| 27S | 0 | 0 | 0 | 7184 | 6773 | 4586 | 2299 | 4579 | 2722 | 3731 | 8861 | 3563 | 1858 | 1126 | 470 | 2342 | 7406 |
| 29S | 0 | 0 | 0 | 6985 | 6962 | 5351 | 3489 | 3748 | 2946 | 7389 | 4766 | 3361 | 1168 | 299 | 462 | 2348 | 6711 |

Fig. 12. Data coverage - ships wind.

# III. LARGE SCALE, LOW FREQUENCY VARIATIONS IN TROPICAL CURRENTS

The physical processes that govern the variability of large scale, low frequency tropical currents (excluding currents at the equator) are believed to be the divergence set up at the surface by the wind stress and the planetary geostrophic divergence inherent on a rotating sphere (Yoshida, 1955; Stommel, 1957; Yoshida and Mao, 1957; Fedorov, 1961; Gill and Niiler, 1973; Meyers, 1975; White, 1977a, b; DeWitt and Leetma, 1978). The emergence of these processes from the equations of motion is shown in the simplest possible way in the model developed below. The necessary distance separating the current from the equator is discussed later.

Consider an ocean with a rigid lid and an infinitely deep bottom layer as shown in Fig. 13. The equations of motion for small perturbations in the upper layer about a state of rest are

$$u_t - fv = -g'h_x + \tau^x/h_o$$

$$v_t + fu = -g'h_y + \tau^y/h_o$$

$$u_x + v_y = h_t/h_o$$

$$g' = \Delta\rho\rho^{-1}g$$

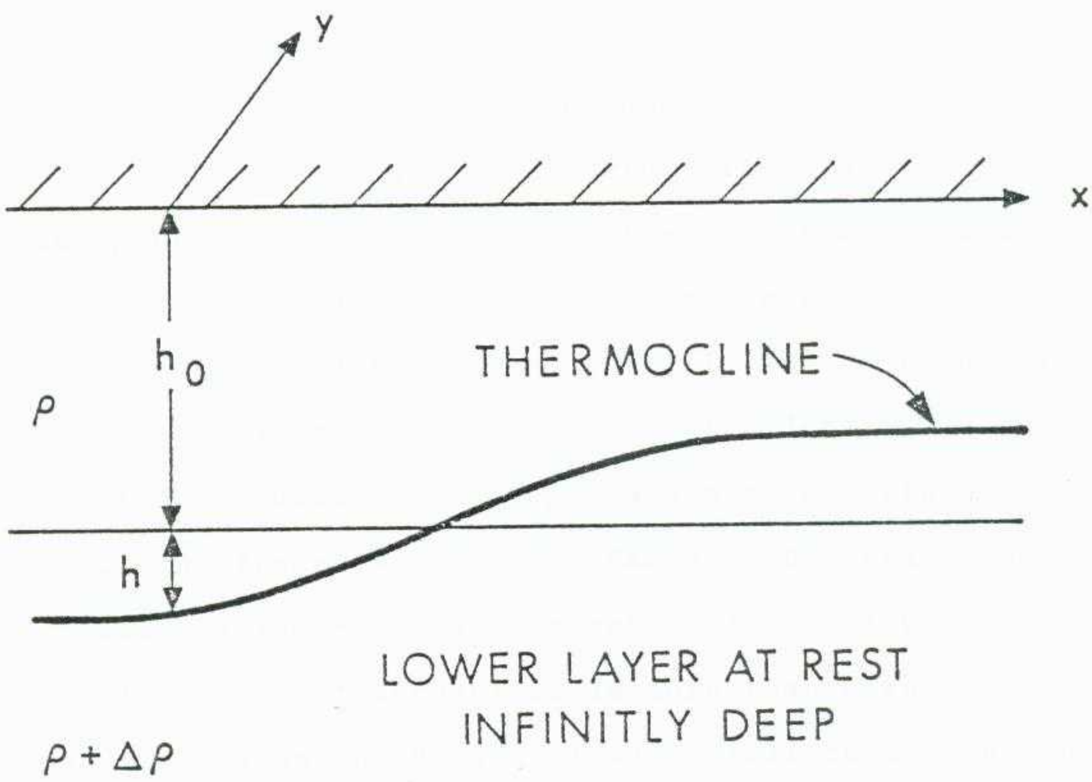


Fig. 13. Two-layer model.

where x and y are horizontal coordinates positive toward the east and the north, u and v are eastward and northward velocity components, subscripts are partial derivatives, f is the Coriolis parameter, g is the acceleration of gravity, $\rho$ is density in the upper layer, $\rho + \Delta\rho$ is density in the lower layer, $\tau^x$ and $\tau^y$ are wind stress toward the east and north, $h_o$ is the thickness of the upper layer when the ocean is at rest, and h is the perturbation in thickness of the upper layer, positive when the interface is displaced downward. Variable currents are nearly in geostrophic balance when their time scale is longer than a few inertial periods and the wind is weak (Bryden, 1977). The fundamental response of the upper ocean to a variable wind stress is the Fredholm solution (Ekman, 1905) which shows that quasi-stationary Ekman currents will develop if the time scale of wind fluctuations is more than a few inertial periods (Greenspan and Howard, 1963). Therefore solutions to the equations of motion with frequency $\omega$ and with $\omega \ll f$ nearly satisfy the momentum equations

$$fv = g'h_x - \tau^x/h_o$$

$$fu = -g'hy + \tau^y/h_o$$

Solving these equations for u and v and substituting into the equation of continuity yields

$$h_t - \frac{\beta g' h_o}{f^2} h_x = -(\frac{\tau^y}{f})_x + (\frac{\tau^x}{f})_y$$

which is the vorticity equation. The local time derivative of vorticity does not appear because it is negligible when the space scale of the motion is large. Scale analysis reveals in detail the conditions under which time variable motion can be described by this vorticity equation, and interested readers are referred to Yoshida and Mao (1957), Phillips (1963, p. 161) and McCreary (1977, p. 22). The approximation filters internal inertio-gravitational waves, Kelvin waves, and short, dispersive Rossby waves from the possible responses of the model. The approximation is not valid near the equator and the required minimum separation from the equator is discussed in the following paragraph. The following transformations yield an equation which will be convenient for later applications. Let

$$h' = -h \qquad\qquad x' = -x$$

$$\mathrm{CURL}_z \frac{\tau}{f} = (\frac{\tau^y}{f})_x - (\frac{\tau^x}{f})_y$$

Then the equation becomes

$$h_t' + \frac{\beta g' h_o}{f^2} h_x' = \mathrm{CURL}_z \frac{\tau}{f}$$

Dropping the primes on h' and x' yields

$$(1) \quad h_t + ch_x = W$$

$$(2) \quad W = \mathrm{curl}_z \frac{\tau}{f}$$

$$(3) \quad c = \frac{\beta g' h_o}{f^2}$$

The rate of change in depth of the thermocline is $h_t$, the Ekman pumping velocity is W, and the planetary geostrophic divergence inherent on a rotating sphere is $ch_x$. Note that derivatives with respect to y (latitude) do not appear in (1) which means that the latitudinal variability in W and c can be incorporated into analytic solutions (White, 1977). Also the x coordinate can be replaced by the distance from the eastern boundary. These features of the model allow for a wide range of flexibility in testing the oceanic responses to meridionally and zonally varying wind fields. A solution to the homogeneous form of (1) which is proportional to $\exp[i(\kappa x-\omega t)]$ where $\kappa$ and $\omega$ are wave number and frequency yields the dispersion relationship for very long, non-dispersive, baroclinic Rossby waves (Veronis and Stommel, 1956, Fig. 1; Lighthill, 1969, Fig. 2)

$$\frac{\omega}{\kappa} = \frac{\beta g' h_o}{f^2}$$

A wind field will generate a large response in the ocean due to resonance when its zonal length scale divided by its time scale nearly equals c. Resonance is discussed further in Chapter 5.

Local accelerations are not negligible at the equator even in low frequency motion. The minimum distance from the equator at which (1) is valid is easily calculated using the equation for meridional velocity (v). This equation will only be used to compare the size of terms derived from accelerations to terms derived from the Coriolis and pressure forces; for simplicity the wind stress is set equal to zero. Taking time derivatives of the momentum equations and substituting for h from the appropriate spatial derivatives of the equation of continuity yields

$$(4) \qquad u_{tt} - f v_t = g' h_o (u_{xx} + v_{xy})$$

$$(5) \qquad v_{tt} + f u_t = g' h_o (u_{xy} + v_{yy})$$

Operating on (4) with $g' h_o \partial^2/\partial x \partial y - f\partial/\partial t$ and on (5) with $\partial^2/\partial t^2 - g' h \partial^2/\partial x^2$ and adding the two resulting equations yields an equation in v alone (Lighthill, 1969),

$$(6) \quad \frac{g'h_o}{f^2}(v_{xx} + v_{yy})_t - \frac{1}{f^2} v_{ttt} - v_t + \frac{\beta g'h_o}{f^2} v_x = 0$$

The terms involving $v_t$ and $v_x$ come from Coriolis and pressure forces. The remaining terms come from local accelerations. Substitution of non-dimensional variables

$$x' = L_x^{-1}x \qquad y' = L_y^{-1}y \qquad t' = \omega t$$

$$v' = v/V^{(s)}$$

yields

$$\frac{g'h_o}{f^2}(L_x^{-2}v'_{x'x'} + L_y^{-2}v'_{y'y'})_{t'} - \frac{\omega^2}{f^2} v'_{t't't'}$$
$$-v'_{t'} + \frac{\beta g'h_o}{f^2}\frac{L_x^{-1}}{\omega} v'_{x'} = 0$$

Consider currents with a zonal length scale

$$L_x = \frac{\beta g'h_o}{\omega f^2}$$

so that the terms involving $v'_{t'}$ and $v'_{x'}$ are the same order of magnitude. For $\omega$ equal to $2\pi/1\text{yr}$, $L_x$ equals 1300 km ($\beta$ and f at 10°N, $g' = 4$ cm $s^{-2}$ and $h_o = 200$ m).

The coefficient of $v'_{x'x't'}$ satisfies

$$\frac{g'h_o L_x^{-2}}{f^2} = \frac{\omega^2 f^2}{\beta^2 g' h_o} \leq .02$$

throughout the tropics, therefore, the term with $v'_{x'x't'}$ is negligible. The coefficient of $v_{t't't'}$ is small everywhere except within a few 10's of kilometers of the equator. The coefficient of $v_{y'y't'}$ is inversely proportional to the square of the Coriolis parameter and increases as the equator is approached. It also increases as the meridional length scale decreases. The smallest meridional length scale apparent in the wind field is 6° of latitude (666 km) as shown in the next chapter. Let the distance from the equator be $\delta_y$ , then f equals $\beta\delta_y$. The coefficient of $v_{y'y't'}$ satisfies

$$\frac{g'h_o L_y^{-2}}{f^2} \leq 0.1$$

when $\delta_y$ is greater than or equal to 584 km. Thus the terms which depend on local accelerations are negligible and (1) is a good approximation if the zonal length scale of the current exceeds 1300 km, the meridional length scale exceeds 666 km and the current is not within 584 km of the equator.

# IV. ANNUAL VARIATION IN THE DEPTH OF THE THERMOCLINE

Annual variation in the strength of the Pacific equatorial currents is expected to be related to the trade winds in the elegantly simple way discussed in Chapter III. The goal of this chapter is to describe the variable currents and trade winds and to test if vertical displacements of the thermocline are in phase with the Ekman pumping velocity computed from the wind stress, or with the Ekman pumping velocity plus the geostrophic divergence as discussed in Chapter III. The test involves comparing the terms in (1) for each month. Given the wind stress and depth of the thermocline in January, the rate of change in depth is calculated at each grid point using (1). The rate of change permits a prediction of the depth for February. The depth for March is similarly calculated from the wind stress and depth of the thermocline observed in February, and so on through the year. In comparing the terms in (1) we will look for agreement in large scale features of the spatial distribution of each term, rather than numerical agreement at each grid point, because the bathythermographic data coverage is not sufficient to calculate long term monthly means with small confidence limits. The results of this test will be given after the annual variations in the depth of the thermocline and the trade winds are described. Note that (1) is singular at the equator; calculations for the region 4°N to 4°S are discussed in Chapter VI.

The trade winds vary during the year with the strongest winds in the winter/spring hemisphere. The wind stress curl and Ekman pumping velocity, however, are relatively insensitive to the changes in wind strength and depend mainly on the locations of the zones of strong meridional shear, which change in latitude throughout the year (Wyrtki and Meyers, 1975a, 1976). The Intertropical Convergence Zone (ITCZ) in the eastern and central Pacific is located about 3° south of its mean position during the northern winter and spring, placing a region of strong cyclonic wind stress curl between 5°N and 10°N (Fig. 14). During the northern summer and fall the ITCZ shifts about 6° northward placing the cyclonic wind stress curl between 10°N and 15°N (Fig. 15). The region south of 10°N is covered by anticyclonic wind stress curl, which is very strong in the eastern Pacific due to the formation of a monsoon wind blowing into Central America (Sadler, 1976). The strongest shear occurs in a narrow band (200-400 km in winter, 400-600 km in summer) just north of the ITCZ and this band passes over the mean position of the ITCZ twice each year; consequently, annual variation in shear is large at the northern and southern limits of the position of the ITCZ and small at the mean position. Another zone of strong cyclonic wind stress curl is located in the south

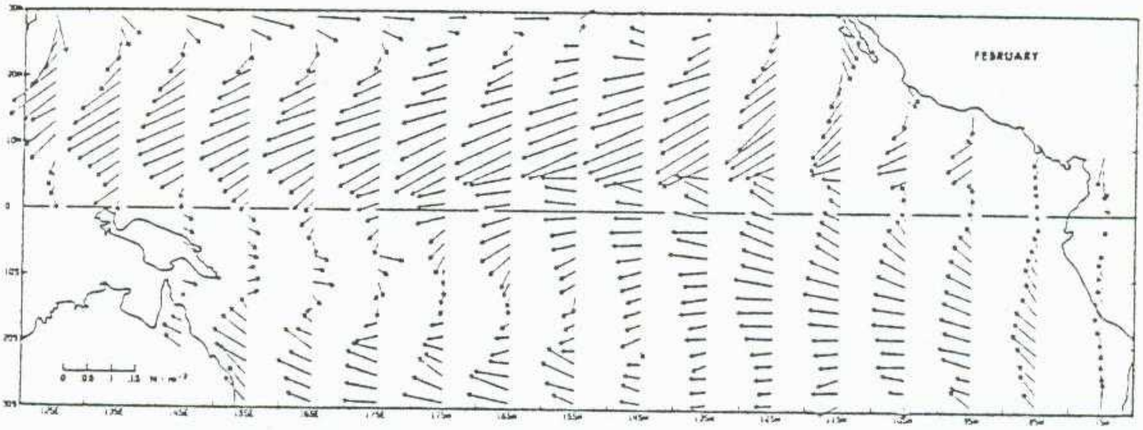


Fig. 14. Wind stress in February.

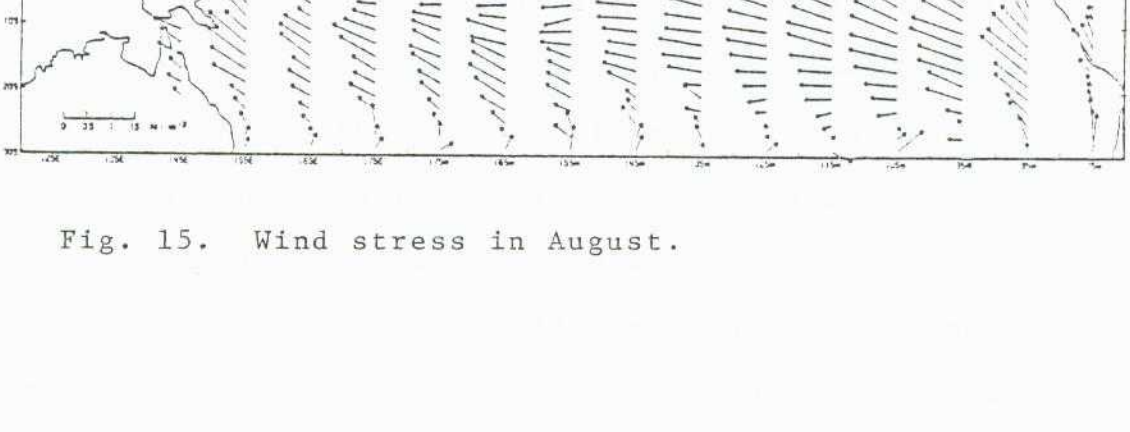


Fig. 15. Wind stress in August.

western Pacific along the southern flank of a trough whose axis runs from the northern Coral Sea to and beyond Fiji during the southern summer (Fig. 14). The trough shifts northward and weakens during the southern winter.

The Ekman pumping velocity (W) in (2) was computed on a 2° latitude by 10° longitude grid. Evaluation of the CURL operator using finite differences has been discussed in Wyrtki and Meyers (1975). Variation in the Ekman pumping velocity throughout the year is described in Fig. 16, which shows a map of the amplitude of the annual harmonic of W. The month during which W attains its maximum value is also shown at a few key locations. Maximum values in the region between 10°N and 15°N occur during August and September across the entire Pacific. The amplitude is very large between 4°N and 8°N in the eastern Pacific with maximum value in March. The fluctuations are not in phase across the Pacific and maximum values occur nearly six months later in the western Pacific. The Ekman pumping velocity in the southwestern Pacific is considerably smaller than in the North Pacific and has a maximum value in February. The spatial structure of the Ekman pumping velocity in the tropical Pacific is by no means simple. Averaging it over longitude or latitude as other investigators have done can be misleading. Consequences of zonal and meridional variation in the forcing will be discussed in the following chapter.

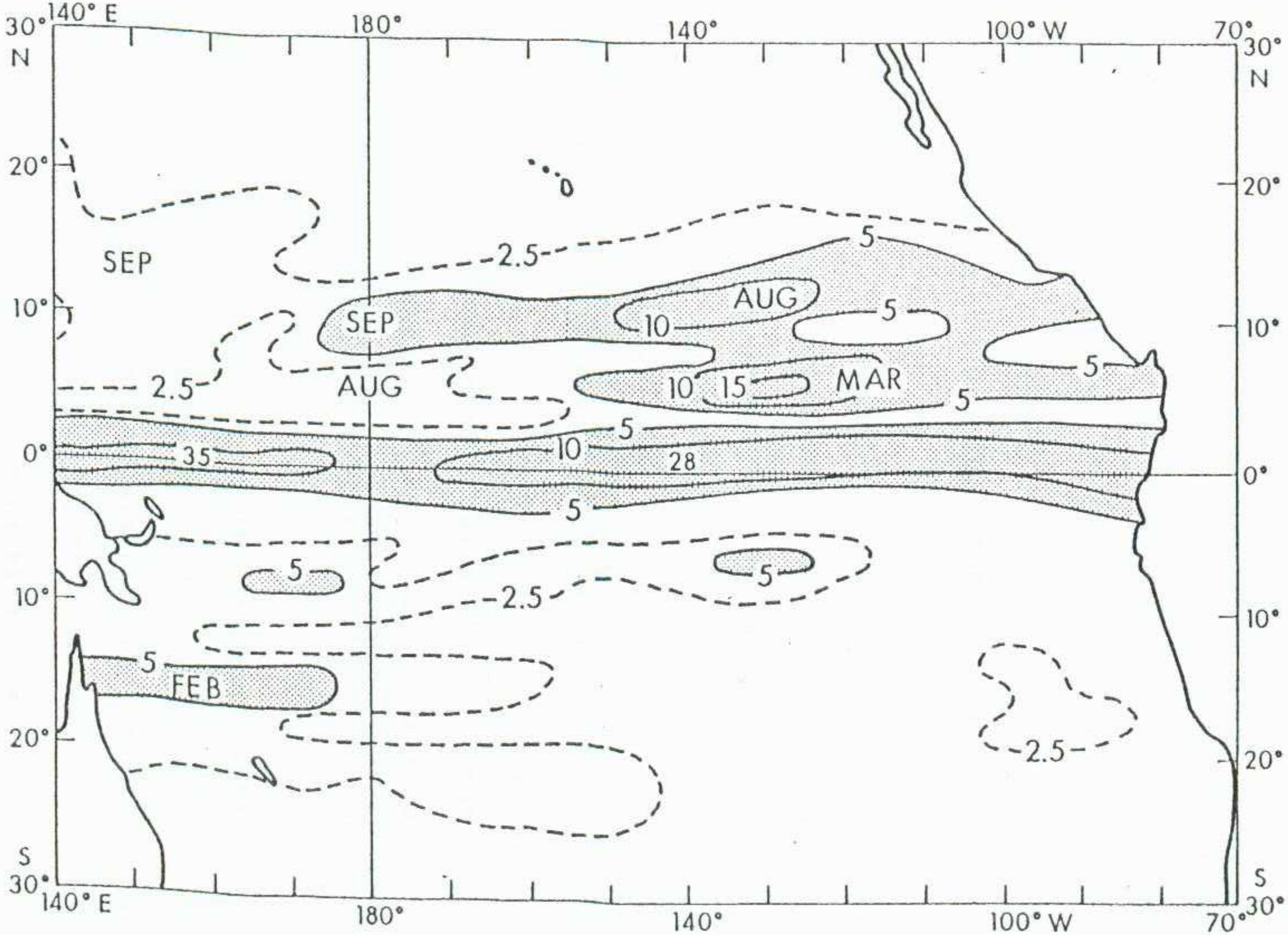


Fig. 16. Annual amplitude of the Ekman pumping velocity in meters per month. The month of maximum upward velocity is given at selected locations.

The observed response of the Pacific equatorial currents to forcing by the trade winds will be discussed next. The tropical Pacific thermocline is characterized by a system of nearly zonally oriented ridges and troughs (Fig. 17) which separate the North Equatorial Current, the North Equatorial Countercurrent and the South Equatorial Current (Knauss, 1962). The countercurrent ridge is located near 10°N between the North Equatorial Current and Countercurrent. The countercurrent trough is located near 5°N between the Countercurrent and the South Equatorial Current. The near equatorial ridges at 2°N and 2°S divide the South Equatorial Current into branches which flow on either side of the equator. The mean structure and its relationship to the Sverdrup transports calculated from the wind stress will be discussed in a separate paper.

The ridges and troughs change in depth throughout the year. The displacement of the thermocline from its mean position during February, May, August and November is shown in Figs. 18 through 21. Arrows on the isolines indicate the direction of inferred changes in geostrophic flow. During November the countercurrent ridge is high across the entire Pacific while the countercurrent trough is deeper than normal in the Central Pacific. Consequently the North Equatorial Current is strengthened across the entire basin while the Countercurrent is greatly strengthened in the Central Pacific. The map also shows strengthening of the

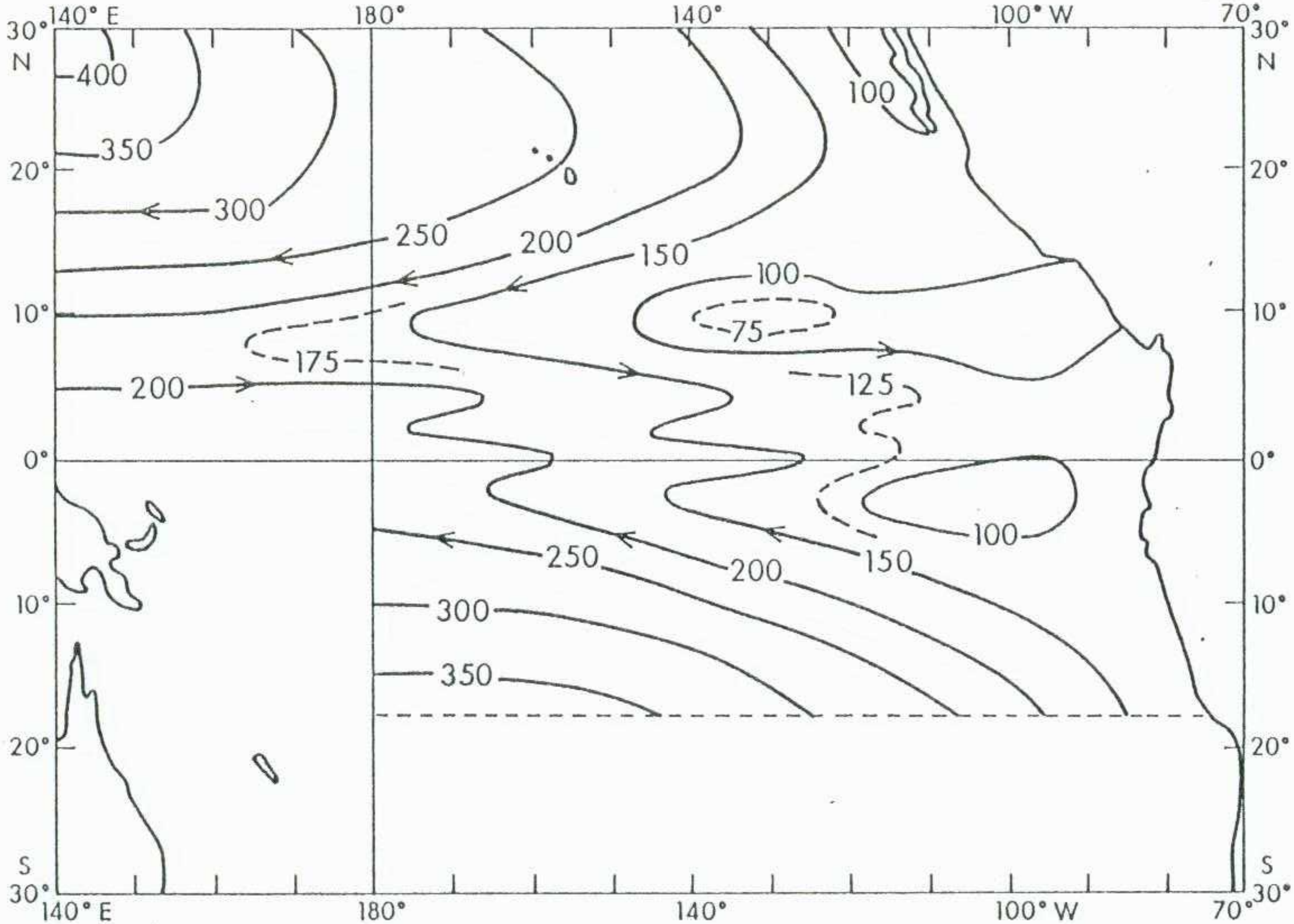


Fig. 17. Mean depth of the 14°C isotherm.

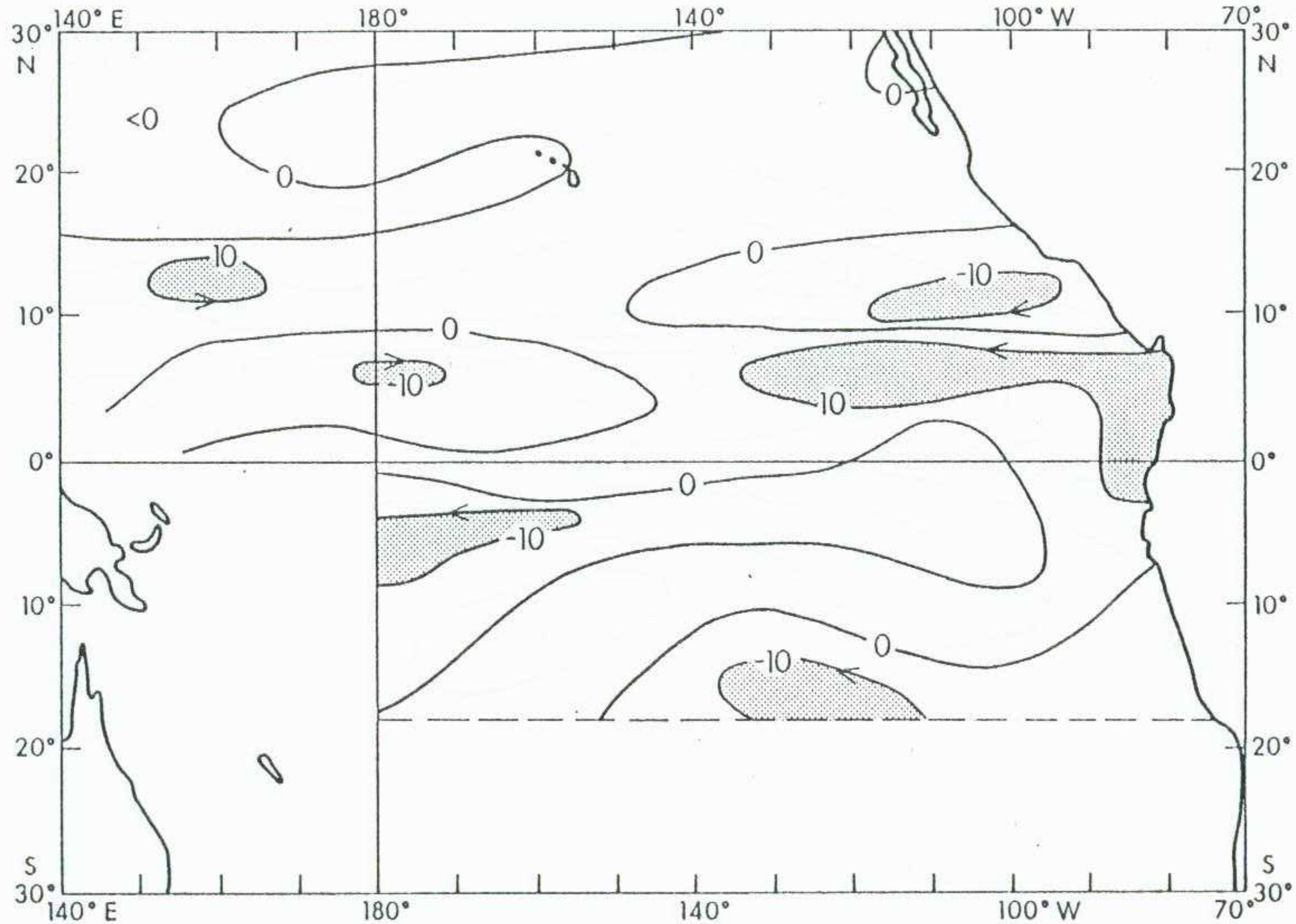


Fig. 18. Displacement of the 14°C isotherm in February.

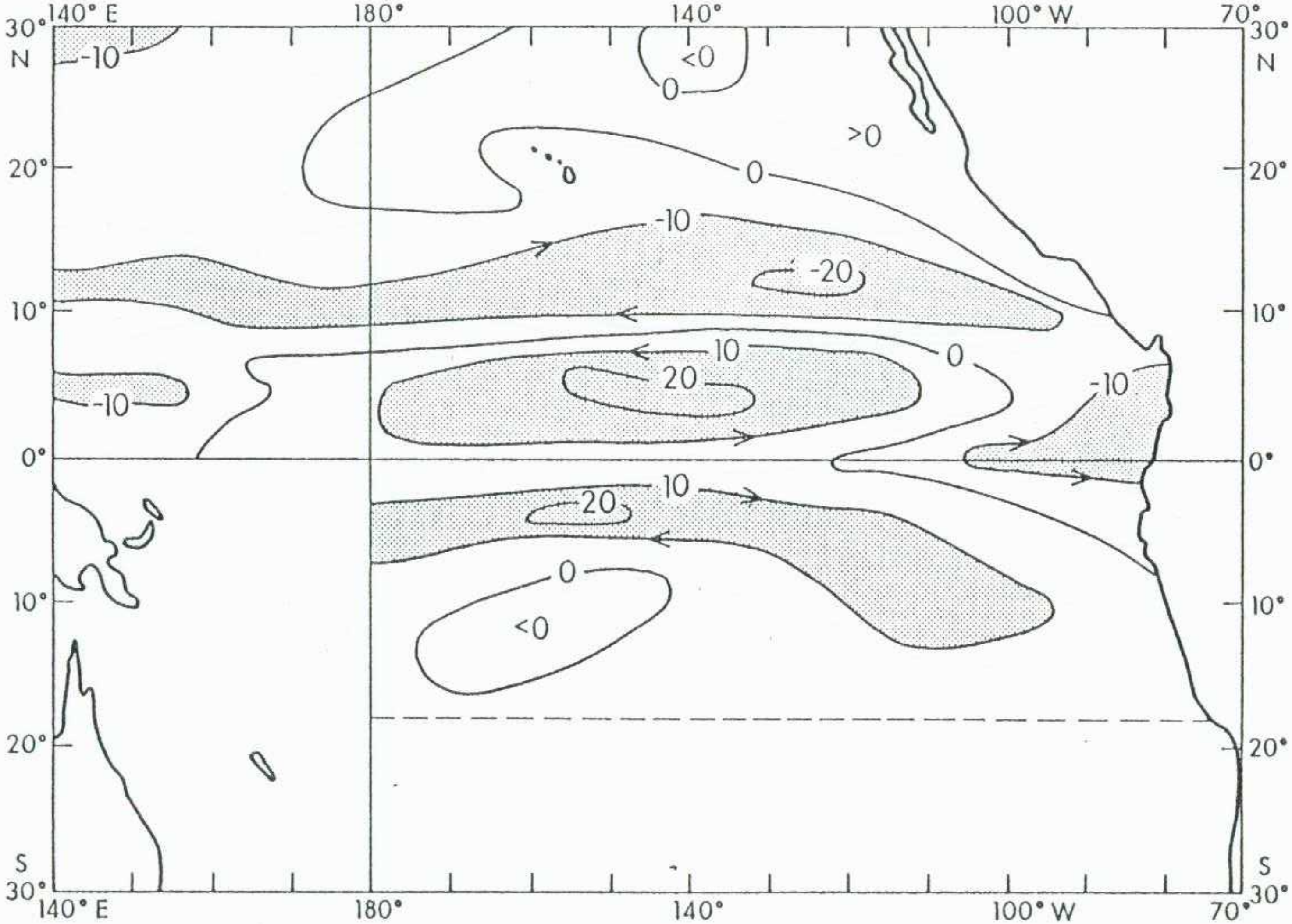


Fig. 19. Displacement of 14°C in May.

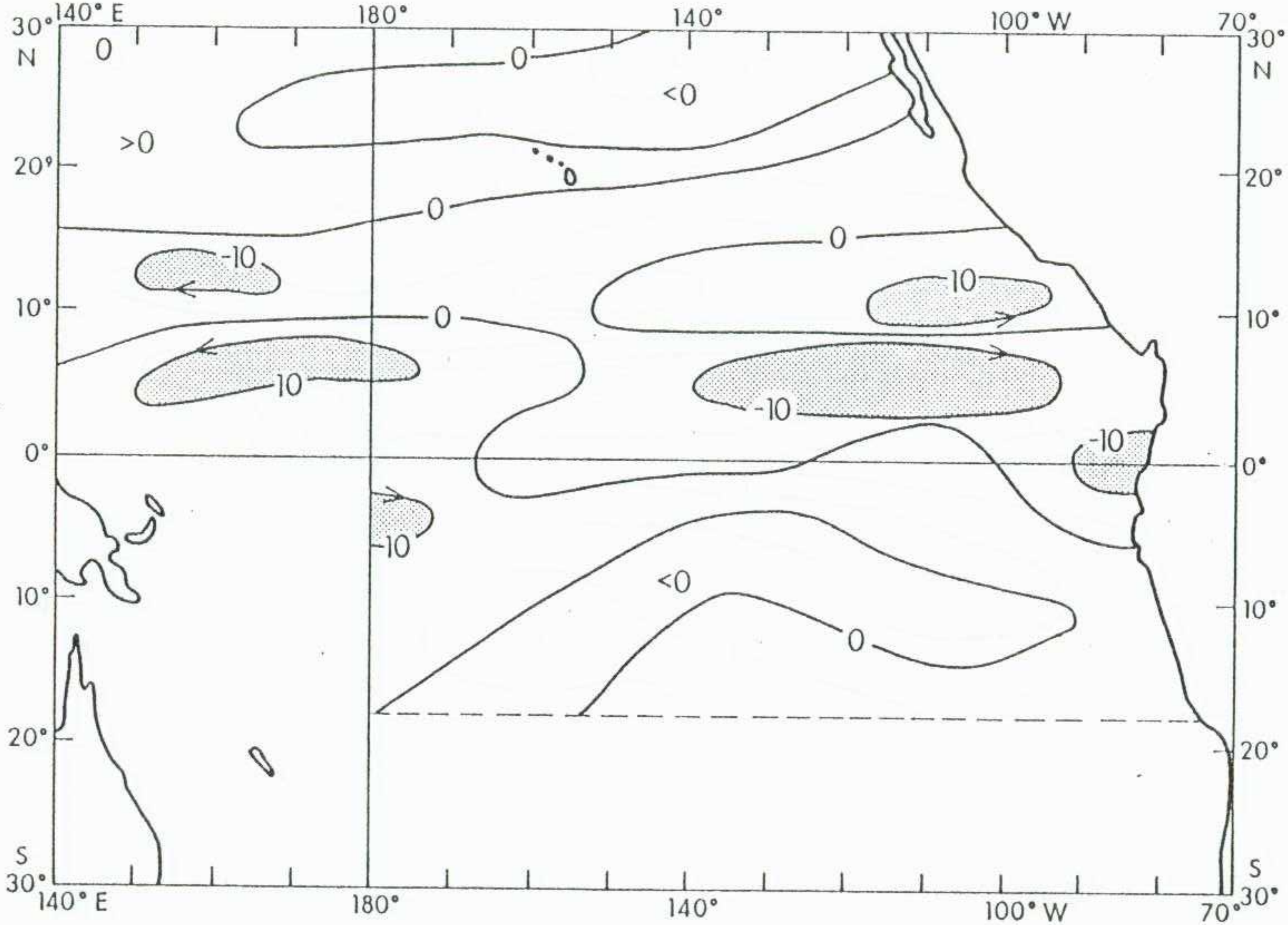


Fig. 20. Displacement of 14°C in August.

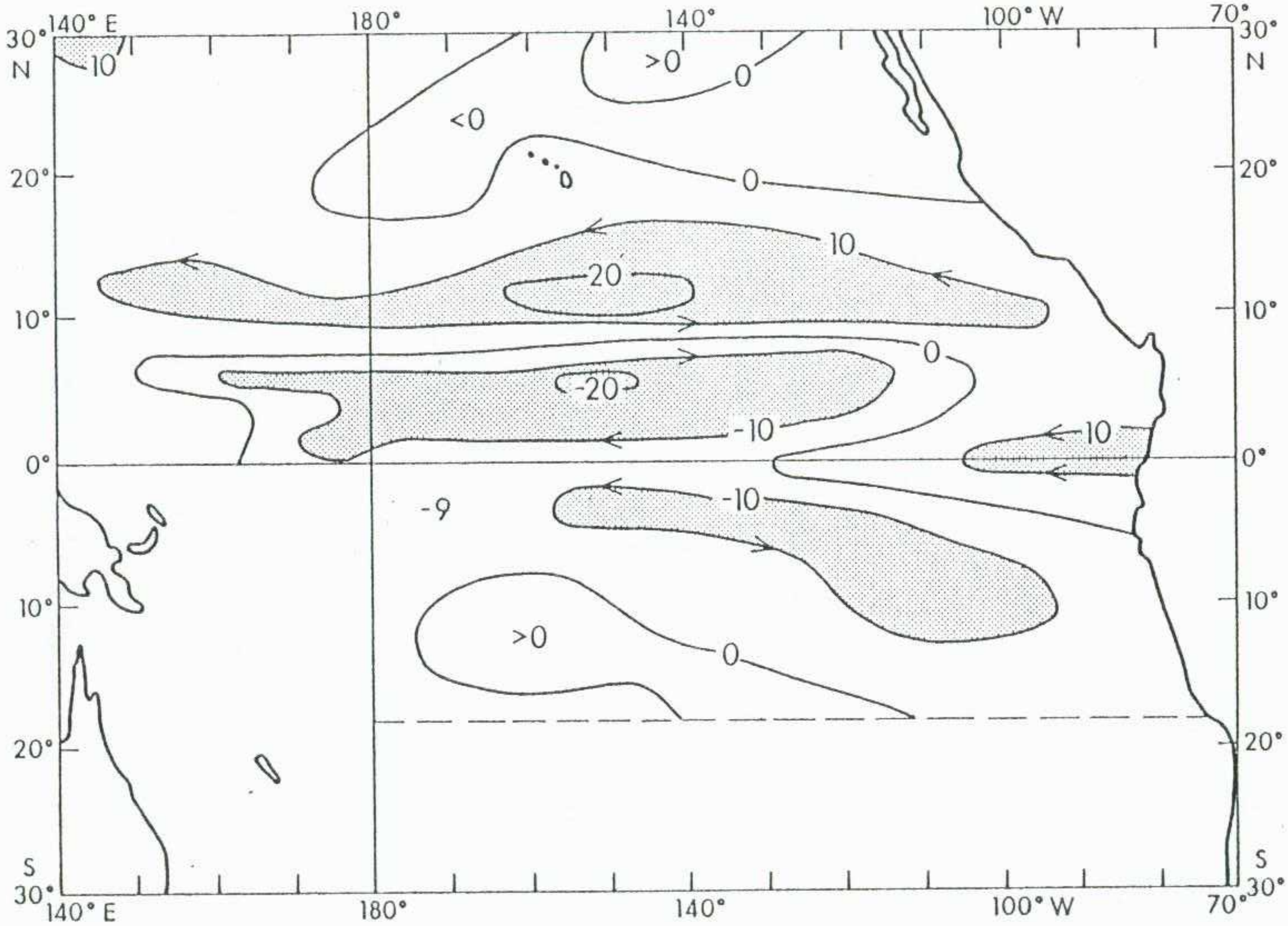


Fig. 21. Displacement of 14°C in November.

South Equatorial Current between about 4°N and 4°S and weakening between 4°S and 10°S. The map for May is almost exactly the reverse of the map for November. The displacements at 6°N propagate westward as seen by following the dome at 115°W in February through the other months. Variation in the depth of the thermocline is summarized in Fig. 22, which shows the amplitude of the annual harmonic of $D_{14}$ throughout the tropical Pacific, and the month of maximum displacement at key locations.

Whether or not these variations in the currents are consistent with the model developed in Chapter III was tested by the following calculations. Monthly displacements ($h_E$) were calculated from the Ekman pumping velocity given in (2) at each grid point by evaluating the integral

$$h_E(t) = \int_o^t W dt' - \langle h_E \rangle$$

The brackets <> indicate the annual mean value. Monthly displacements ($h_G$) were also calculated from the geostrophic divergence in (3) by evaluating

$$h_G(t) = \int_o^t c h_x dt' - \langle h_G \rangle$$

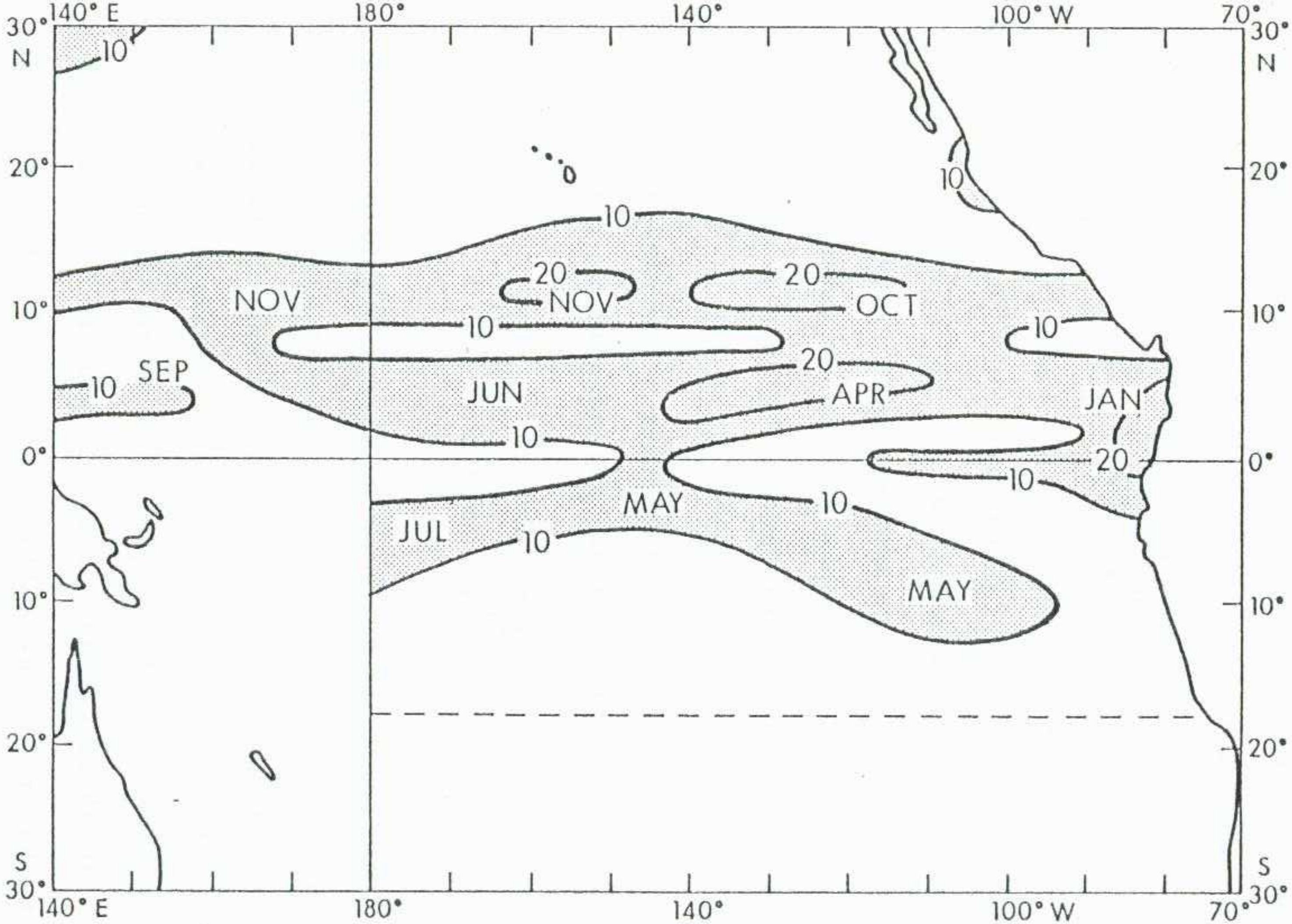


Fig. 22. Annual amplitude of the depth of the 14°C isotherm. The month of maximum upward displacement is given at selected locations.

The calculated anomalies $h_E$ (t) and $h_E$ (t) + $h_G$ (t) were compared to the observed anomalies (h) at each grid point by calculating the correlation coefficient for the twelve monthly values. The correlation coefficient of two sinusoidal curves, cos $\omega t$ and cos $(\omega t + \phi)$, is cos $\phi$, and equals .87 if the lag $\phi$ equals 1 month. Areas where the correlation coefficient between $h_E$ and h exceeded .87 is shown in Fig. 22. The figure indicates that the Ekman pumping velocity is in phase with vertical displacements of the thermocline in the region between 10°N and 15°N across the Pacific from the eastern boundary to 155°E. The correlation coefficient does not give any information about the agreement in magnitude of the anomalies. This was evaluated by calculating the ratio (R')

$$R' = \frac{1}{12} \sum_{i=1}^{12} \frac{(h_i' - h_i)^2}{h_i^2}$$

where h' is either $h_E$ (t) or $h_E$ (t) + $h_G$ (t). The value of R' is zero if the compared quantities are exactly equal and increases in size as the difference between the compared quantities increases. The average value of R' in the region where the Ekman pumping velocity and displacements of the thermocline are in phase is .22. The magnitude of a typical displacement is 15 m, which implies that a typical error ($\varepsilon$) is 7 m as shown in the calculation below.

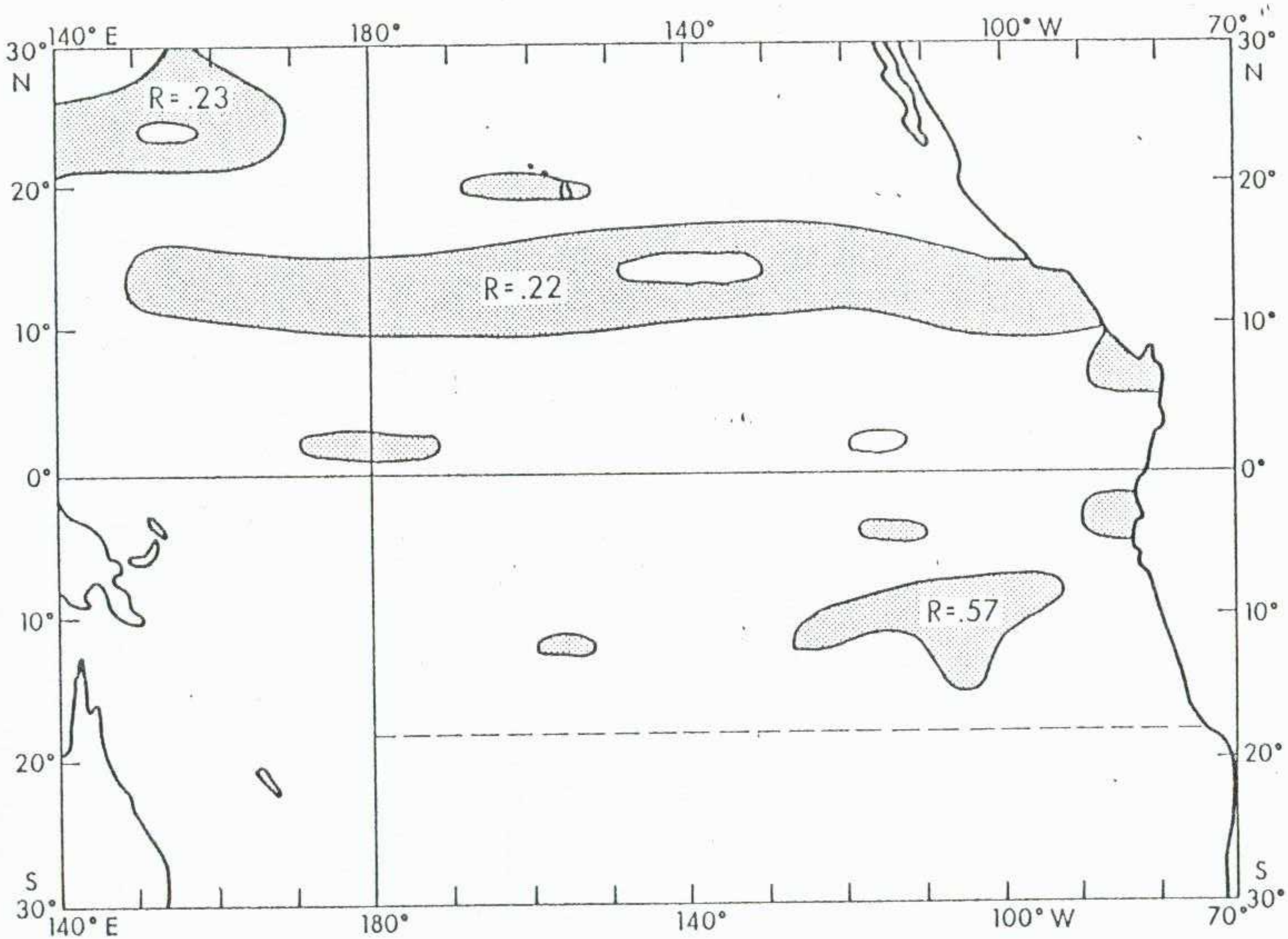


Fig. 23. Region where the rate of change in depth of 14°C is in phase with the Ekman pumping velocity, determined by a method explained in the text.

$$\varepsilon = (.22 \times 15^2)^{\frac{1}{2}}$$

Excluding small isolated spots, three smaller areas of phase agreement are found centered at 24°N, 155°E in the western Pacific, at 10°S, 105°W in the eastern Pacific and at 20°S and the dateline. Notably absent from the regions of phase agreement is the area between 4°N and 8°N which has both large observed displacements and Ekman pumping velocities. Addition of the geostrophic divergence yields calculated displacements $h_E$ (t) + $h_G$ (t) which are in phase with observed displacements throughout most of the region from 4°N to 15°N (Fig. 24). The implication is that the annual variations in strength of the North Equatorial Current and the Countercurrent are consistent with a model that incorporates Ekman pumping and geostrophic divergence. Models which incorporate more terms in the vorticity equation can be developed; however, these two processes are fundamental and will be active in any model.

To summarize the results presented in this chapter, vertical displacements of the thermocline between 10°N and 15°N are in phase with the Ekman pumping velocity, while from 4°N to 6°N they are in phase with the Ekman pumping velocity plus the geostrophic divergence. We might ask why the response is different at these two latitudes. The

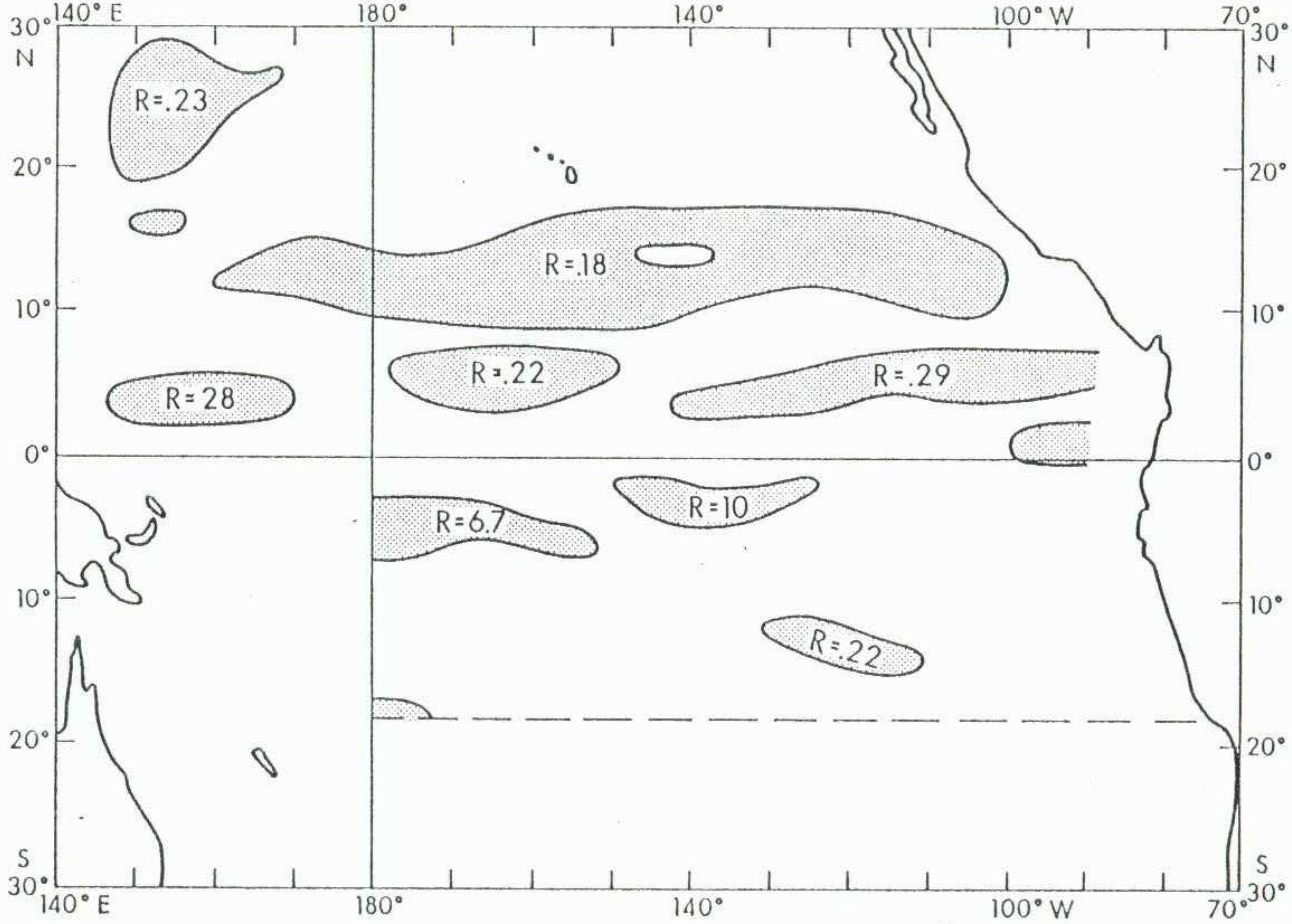


Fig. 24. Region where the rate of change in depth of 14°C is in phase with the Ekman pumping velocity plus the geostrophic divergence, determined by a method explained in the text.

answer probably concerns the structure of the wind field. The Ekman pumping velocity has equal phase across the Pacific at 10°N; it shifts in phase nearly half a year at 6°N. The amplitude at 6°N also has a larger zonal variability than at 10°N. The ocean's response to these variations in the wind field is discussed in the next chapter.

# V. ON THE ANNUAL ROSSBY WAVE IN THE TROPICAL NORTH PACIFIC

Vertical displacements of the thermocline are in phase with the Ekman pumping velocity plus the geostrophic divergence in the region between 4°N and 15°N. The best resolution of the annual signal was achieved in this region because the annual amplitude of the displacements in it is larger than anywhere else in the tropical Pacific. We are encouraged to investigate this region in greater detail. In the last chapter the mean topography of the thermocline in January (an initial condition) and the Ekman pumping velocity were used to calculate the topography of the thermocline in February. The observed topography for February was then introduced as a new initial condition to calculate the topography for March. Calculations for the full year required 12 initial conditions. It is possible to solve (1) for an arbitrary forcing function using only one initial condition and a boundary condition. These solutions can be called forced baroclinic Rossby waves because the free sinusoidal solutions are the well known, non-dispersive Rossby waves discussed by Veronis and Stommel (1956) and Lighthill (1969). In this chapter solutions to (1) for idealized wind fields are used to show their general properties. Then a solution for a forcing function which closely approximates the observed wind field is found and compared to observations. The solutions discussed in this chapter show why the oceanic response at 10°N is dominated by local Ekman pumping while the response at 6°N propagates westward and geostrophic divergence is not negligible.

The general solution to (1) is the sum of a particular solution plus the solution to the homogeneous equation. The general solution of the homogeneous equation is

$$h = h(x-ct)$$

Given an initial condition

$$h_i(x) = h(x,0)$$

the solution to the homogeneous equation for all subsequent time is

$$h(x,t) = h_i(x-ct)$$

which represents non-dispersive westward propagation of the initial topography. The ocean has an eastern boundary at $x = 0$, therefore $h_i(x)$ is not defined for $x<0$ and the solution $h(x,t)$ for $x<ct$ is also not defined. The existence of a solution for $x>ct$ is represented in Fig. 25 which shows the characteristic of the differential equation and the initial condition. It is clear that the initial condition influences the solution only in the part of the x,t

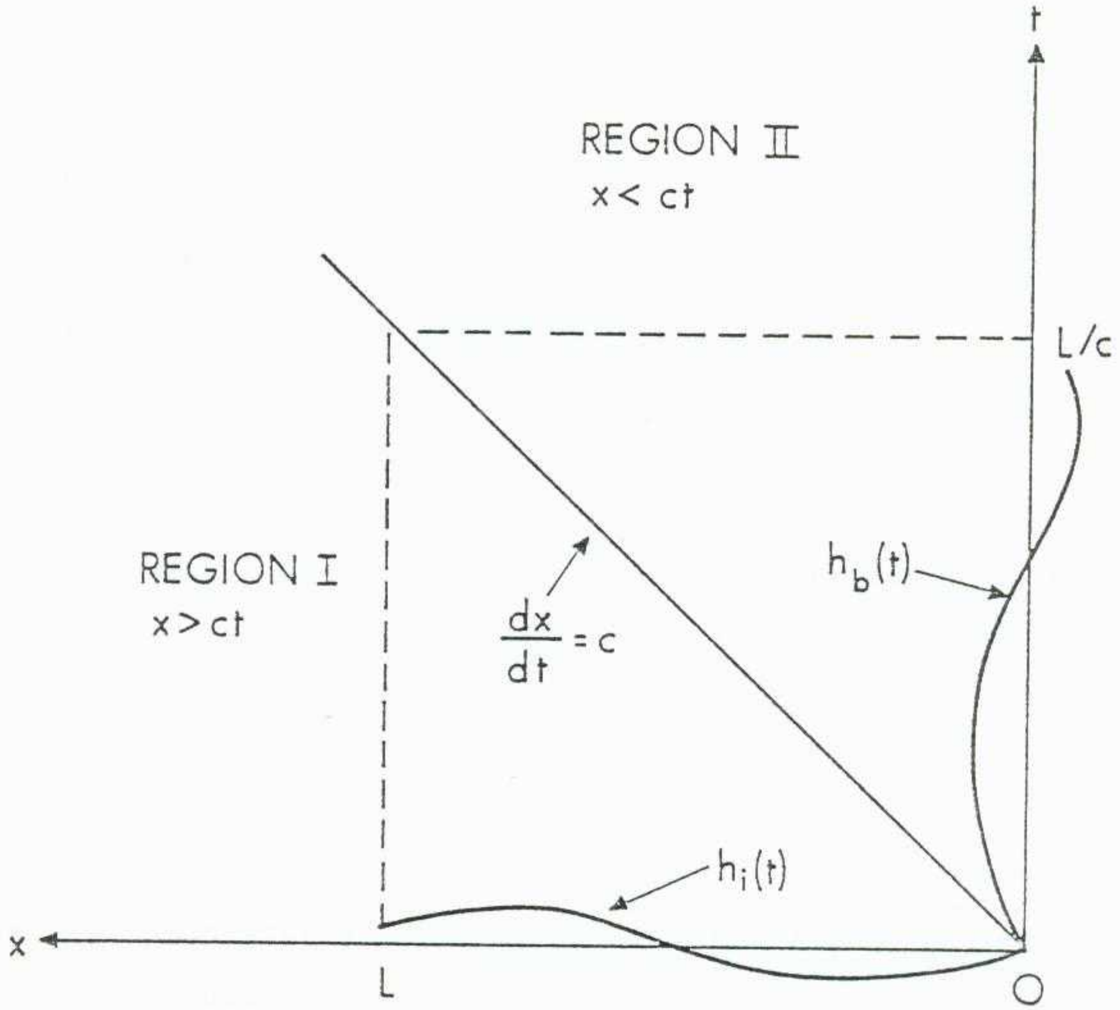


Fig. 25. Characteristics of equation (1).

space where $x>ct$ (region I). A solution in the part where $x<ct$ (region II) requires a boundary condition

$$h_b(t) = h(0,t)$$

The solution to the homogeneous equation in this case is written in the form

$$h(x,t) = h(t - \frac{x}{c})$$

For the boundary condition the solution is

$$h(x,t) = h_b\ (t - \frac{x}{c})$$

which represents non-dispersive westward propagation of the boundary condition. If a solution to (1) is sought for a limited part of the ocean, say for

$$L \geq x \geq 0$$

then Fig. 25 suggests that the initial condition influences the solution until t equals L/c and subsequently the solution depends only on the boundary condition. The solutions discussed below are all in region II, and depend only on the eastern boundary condition.

White (1977) solved (1) but his solution does not represent the observations. He used the idealized forcing function

$$W = A \cos \omega t$$

and the boundary condition

$$h_b(t) = 0$$

The solution is

$$(7) \qquad h = \frac{2A}{\omega} \sin(\frac{\kappa x}{2}) \cos(\frac{\kappa x}{2} - \omega t)$$

Observed displacements of the thermocline in a small area of the Central Pacific were used to evaluate A and the phase. White (1977) then used (7) to calculate a map of the amplitude and phase of the annual wave throughout the tropical North Pacific (Fig. 26). This wave propagates through the amplitudinal envelope (Fig. 26B) at twice the phase speed of a baroclinic, non-dispersive Rossby wave. The observed topography of the thermocline throughout the tropical Pacific shown in Figs. 18 through 21 shows that the fluctuations at 10°N have nearly the same phase across the Pacific from the eastern boundary to 145°E. The wave suggested by White (1977) shifts in phase by a full cycle over this range of longitude (Fig. 26A). The wave shown in Fig. 26 is therefore not present.

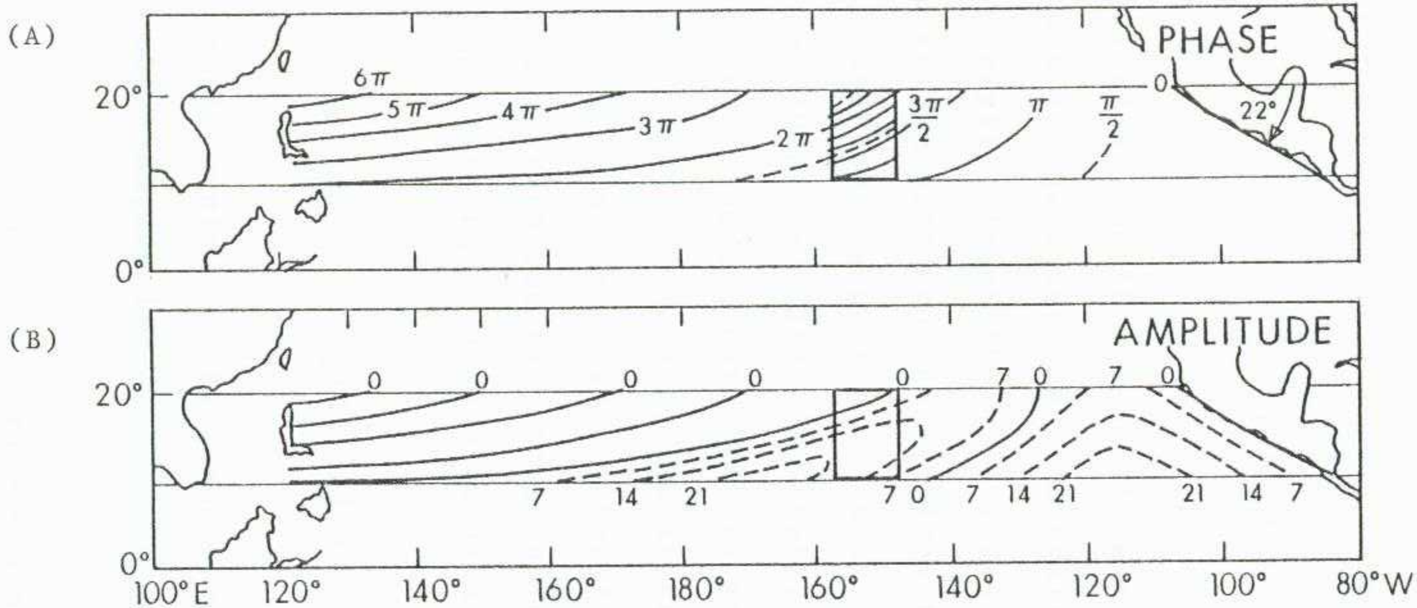


Fig. 26. The annual Rossby wave according to White (1977).

The solution (7) is only one of the possible solutions to (1). Others can be found by altering the forcing function and the boundary condition. The condition

$$h_b(t) = 0$$

is the logical one if the model uses quasi-geostrophic equations at the coastline. In reality local accelerations are not negligible at the coast, and the accelerations permit Kelvin waves to travel along the coast. Packets of these waves can change the depth of the thermocline along the coast (McCreary, 1976; Hurlburt, 1976). Without resorting to a more complex mathematical model (1) can be solved using the observed boundary condition at some distance far enough away from the coast so that local accelerations are negligible. With the same forcing function as in White (1977) and with the boundary condition changed to

$$h_b(t) = \int_o^t W dt$$

(i.e. local forcing by the Ekman pumping velocity near the coast) the solution is

$$(8) \qquad h(x,t) = \frac{A}{\omega} \sin \omega t$$

In this solution the displacements of the thermocline are in phase with the Ekman pumping velocity across the entire ocean. A resonant response of the system is found by letting the forcing function be

$$W = A \sin(\kappa x) \cos(\omega t)$$

with $\kappa$ almost equal to $\omega/c$. The solution for constant boundary condition is

$$(9) \qquad h(x,t) = \frac{A}{2c(\kappa - \omega c^{-1})} \left[\cos\left(\omega t - \frac{\omega x}{c}\right) - \cos(\omega t - \kappa x)\right]$$

neglecting small terms, which are not divided by the factor $\kappa - \omega/c$. The response becomes very large as $\kappa - \omega/c$ becomes small. Thus a system governed by (1) can yield

1. a forced wave which propagates at twice the phase speed of a free non-dispersive Rossby wave as in (7).
2. a local response forced by the Ekman pumping velocity as in (8) or
3. large amplitude, resonant waves which propagate at nearly the phase speed of a free non-dispersive Rossby wave as in (9).

Solutions for the observed wind field will now be studied to look for properties 1) through 3) and also they will be compared to the observed variations.

For an arbitrary forcing function $W(x,t)$, an arbitrary boundary condition $h_b(t)$, and the initial condition $h_i(x,o) = 0$, the Laplace transform of the solution is

$$H(k,s) = \frac{w(k,s)}{(kc + s)} + \frac{cH(o,s)}{(kc + s)}$$

where k is the transform parameter for x, s is the transform parameter for t, $w(k,s)$ is the forcing function transformed in space and time and $H(o,s)$ is the boundary condition transformed in time. Inverse transformation in k and application of the convolution theorem yield

$$H(x,s) = \frac{1}{c} \int_o^x e^{-\frac{s}{c}(x-\zeta)} w(\zeta,s)\, d\zeta + H(o,s)\, e^{-\frac{s}{c}x}$$

Inverse transformation in s and another application of the convolution theorem yield

$$h(x,t) = \frac{1}{c} \int_o^x \int_o^t \delta[t - \tau - \frac{(x-\zeta)}{c}]\ W(\zeta,\tau)\, d\tau d\zeta$$

$$+ \int_o^t \delta[t - \tau - \frac{x}{c}]\ h_b(\tau)\, d\tau$$

where $\delta$ is the Dirac-delta function. The solution in region II of Fig. 25 ($x<ct$) is independent of the initial

condition. After a time interval L/c the solution yields values of h across the ocean from the origin to L for all subsequent time. Using the inequalities

$$t - \frac{(x-\zeta)}{c} > 0$$

$$\zeta \geq 0$$

$$\tau \leq t$$

and properties of the Dirac-delta function, the integral over $\tau$ can be evaluated to yield the solution

$$(10) \qquad h(x,t) = \frac{1}{c} \int_0^x W[\zeta, t - \frac{(x-\zeta)}{c}] d\zeta + h_b \left(t - \frac{x}{c}\right)$$

The observed Ekman pumping velocity can be very closely represented by a function of the form

$$W = A(x) \cos(\omega t) + B(x) \sin(\omega t)$$

A(x) and B(x) are the annual harmonic Fourier coefficients of the observed Ekman pumping velocity. They are piece-wise-continuous, linear functions between grid points. The forcing function is then specified by

$$A(x) = \begin{cases} \gamma_1{}^1 x + \gamma_2{}^1 & \alpha^2 \geq x \geq \alpha^1 \\ \gamma_1{}^2 x + \gamma_2{}^2 & \alpha^3 \geq x \geq \alpha^2 \\ \cdot & \\ \cdot & \\ \cdot & \\ \gamma_1{}^N x + \gamma_2{}^N & \alpha^{N+1} \geq x \geq \alpha^N \end{cases}$$

$$B(x) = \begin{cases} \gamma_3{}^1 x + \gamma_4{}^1 & \alpha^2 \geq x \geq \alpha^1 \\ \gamma_3{}^2 x + \gamma_4{}^2 & \alpha^3 \geq x \geq \alpha^2 \\ \cdot & \\ \cdot & \\ \cdot & \\ \gamma_3{}^N x + \gamma_4{}^N & \alpha^{N+1} \geq x \geq \alpha^N \end{cases}$$

where the $\gamma^i$ are calculated from the harmonic coefficients at points on the x-axis $\alpha^1$, $\alpha^2$, $\alpha^3$, ... , $\alpha^N$, $\alpha^{N+1}$. A tedious but otherwise straight forward integration of (10) with this forcing function yields

$$(11) \quad h(x,t) = \sum_{i=1}^{M} [C_i(x,t) + S_i(x,t)] + h_b\ (t - \frac{x}{c})$$

$$\alpha^{M+1} \geq x \geq \alpha^{M}$$

$$C_i(x,t) = \frac{1}{c}\ [\frac{\gamma_1^{\ i}}{\kappa^2}\ (\cos\eta + \kappa\zeta\sin\eta) + \frac{\gamma_2^{\ i}}{\kappa}\ \sin\eta]_{\eta=\eta_i,\ \zeta=\alpha^i}^{\eta=\eta_{i+1},\ \zeta=\zeta^{i+1}}$$

$$S_i(x,t) = \frac{1}{c}\ [\frac{\gamma_3^{\ i}}{\kappa^2}\ (\sin\eta - \kappa\zeta\cos\eta) - \frac{\gamma_4^{\ i}}{\kappa}\ \cos\eta]_{\eta=\eta_i,\ \zeta=\alpha^i}^{\eta=\eta_{i+1},\ \zeta=\alpha^{i+1}}$$

$\kappa = \omega/c$

$\eta = \omega t - \kappa x + \kappa\zeta$

$\eta_i = \omega t - \kappa x + \kappa\alpha^i$

$\alpha^{M+1} = x$

The non-dispersive Rossby wave phase speed

$$c = \frac{\beta g' h_o}{f^2}$$

must be evaluated before calculating displacements of the thermocline from (11). Observed displacements at 6°N plotted as a function of longitude and time (Fig. 27) suggest a phase speed of about 64 cm $s^{-1}$ (represented by a line in the lower left portion of the figure). The solution (11) with this phase speed and the observed boundary condition at 80°W is shown in Fig. 28. The solution propagates westward at the free wave phase speed and has a large amplitude (>60m). The half-wave length corresponding to the wave number $\omega/c$ (with $\omega = 2.10^{-7}$ $s^{-1}$ and $c = 64$ cm $s^{-1}$) is $1.0 \times 10^4$ km, or 91° of longitude at 6°N. This half-wave corresponds to the distance from 160W to the American coast, and traverses a distinct maximum in the spatial distribution of the Ekman pumping velocity (Fig. 16 ). Also the Ekman pumping velocity in the eastern and western Pacific is 6 months out of phase. It appears that the westward propagating wave at 6°N is a nearly resonant response of the ocean to the zonal distribution of the Ekman pumping velocity as in case 3. The calculated displacements are three times larger than the observed displacements at least partly because both dissipation and dispersive transport of energy to other latitudes are not permitted by the

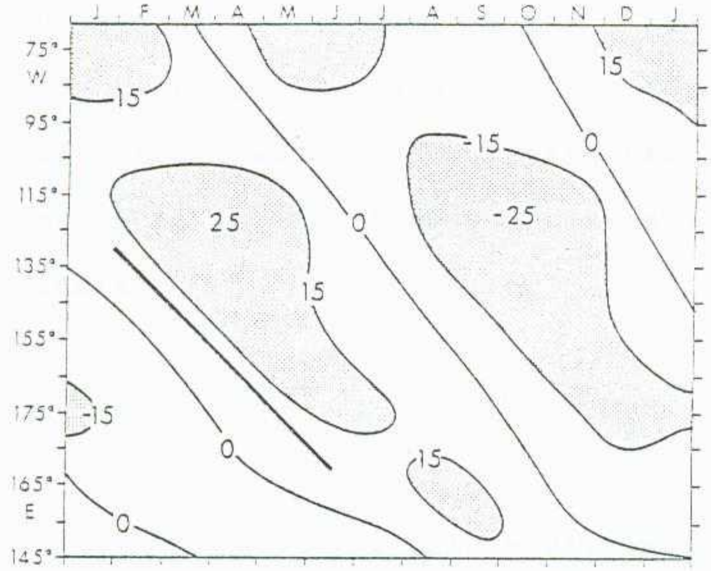


Fig. 27. Observed depth of 14°C at 6°N.

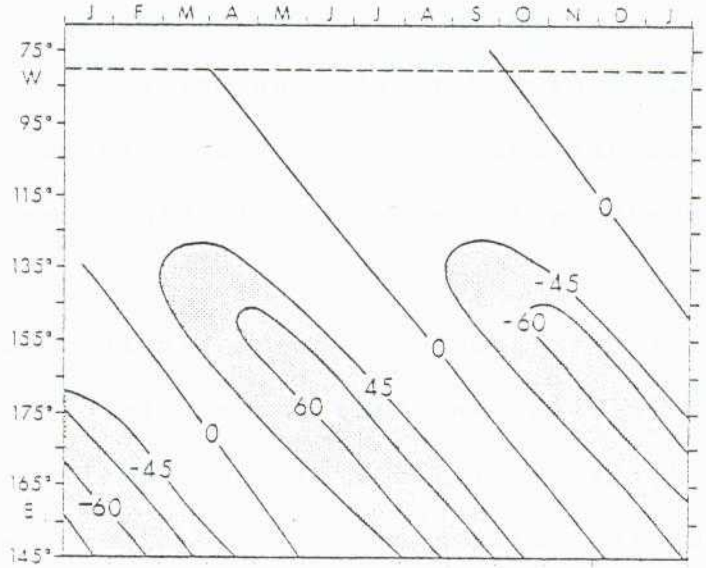


Fig. 28. Calculated depth of 14°C at 6°N.

differential equation (1).

The phase speed c can be calculated from the density structure through its dependence on $g'h_o$, and it is possible to test if the value estimated above ($c = 64$ cm $s^{-1}$) is consistent with the observed density structure. The quantity $g'h_o$ can be calculated from oceanographic station data with the formula

$$g'h_o = gH^{(1)}$$

where $H^{(1)}$ is the first baroclinic equivalent depth. The physical meaning and calculation of $H^{(1)}$ has been discussed in detail by Lighthill (1969, p. 85 ff.). Near 6°N $H^{(1)}$ is 53 cm at 129°W and 83 cm at 160°W, as calculated from the oceanographic station data described in Table 1. The phase speed calculated from the mean equivalent depth is 65 cm $s^{-1}$, which is remarkably close to the value determined from Fig. 27.

Observed displacements of the thermocline at 10°N as a function of longitude and time have nearly the same phase from the American coast to 145°E (Fig. 29). The figure does not suggest a value for c. Subtraction of the zonal mean displacement each month shows that relatively small westward propagating features with a phase speed of 56 cm $s^{-1}$ are hidden beneath the large zonally uniform signal (Fig. 30).

| LATITUDE | LONGITUDE | $H^{(1)}$ | DATA SOURCE | EXPEDITION |
|---|---|---|---|---|
| 6°N | 160°W | 83(cm) | Reid (1965) | Equapac |
| 10°N | 160°W | 53 | | |
| 18°N | 160°W | 90 | | |
| 7°N | 129°W | 53 | Reid *et. al.* (1965) | Downwind |
| 11°N | 128°W | 51 | | |
| 19°N | 125°W | 57 | | |

Table 1. First baroclinic equivalent depth $H^{(1)}$.

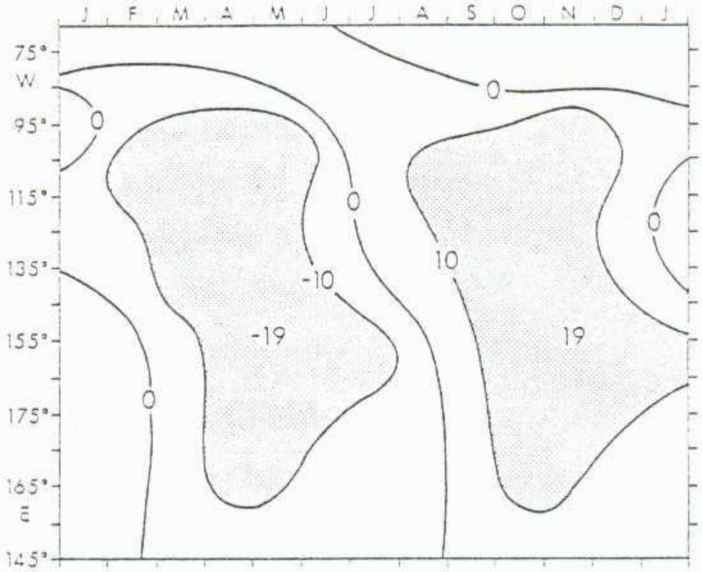


Fig. 29. Observed depth of 14°C at 10°N.

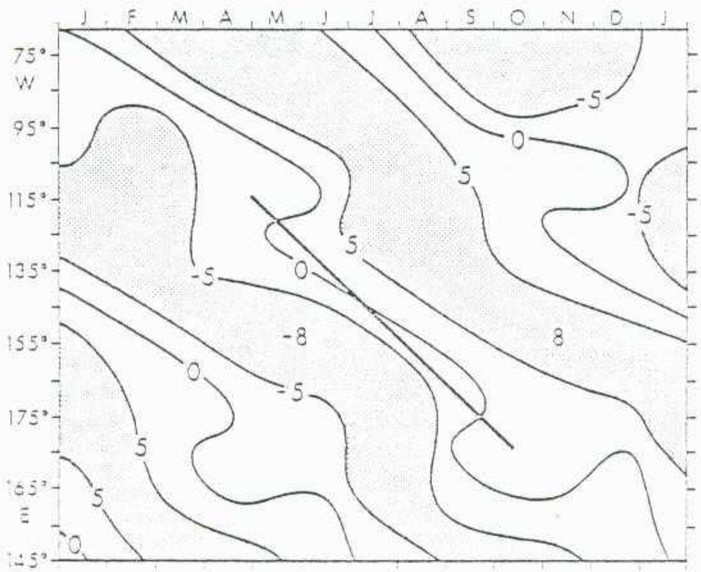


Fig. 30. Observed depth of 14°C at 10°N minus the monthly zonal mean.

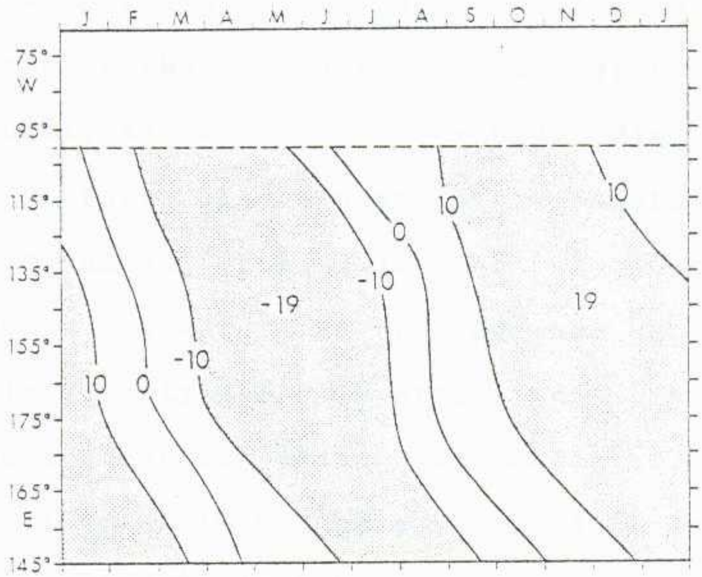


Fig. 31. Calculated depth of 14°C at 10°N.

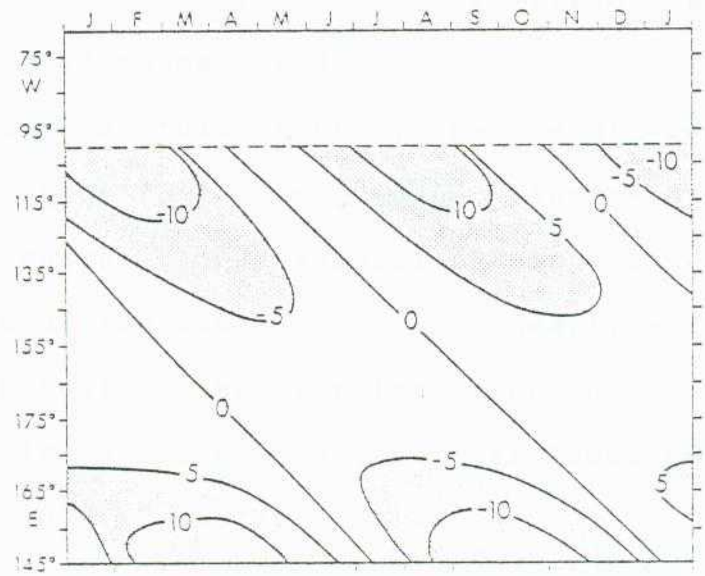


Fig. 32. Calculated depth of 14°C at 10°N minus the monthly zonal mean.

The solution (11) with $c = 56$ cm $s^{-1}$, and with the observed forcing function at 10°N and the observed boundary condition at 100°W is shown in Fig. 31. The figure suggests a local response in the thermocline forced by the Ekman pumping velocity as in case 2. The underlying westward propagating features also appear in the solution when the zonal mean is removed (Fig. 32). The solution at 10°N is weakly dependent on the value of c because geostrophic divergence is of only minor importance at this latitude. A complication is that the phase speed calculated from the density structure at 10°N does not exceed 20 cm $s^{-1}$ using the mean value of $H^{(1)}$ in table 1. Perhaps a model which includes the meridional transport of energy, mean currents, and a more realistic vertical density structure can account for the observed phase speed.

In summary of this chapter, the oceanic response at 6°N to forcing by the Ekman pumping velocity takes the form of a nearly resonant non-dispersive Rossby wave because the length scale of the free Rossby wave nearly matches the zonal length scale of the forcing function. At 10°N the thermocline is in phase with the local Ekman pumping velocity from 100°W to 145°E.

# VI. THE REGION BETWEEN 4°N AND 4°S

The equator is a singular region where quasi-geostrophic dynamics breaks down, and the model developed in Chapter III is not applicable. The Ekman pumping velocity in the region between 4°N and 4°S was computed with a simple model that is consistent with the dynamics of equatorial currents. The wind stress must be balanced by friction at the equator, as has been discussed in a conceptual model by Cromwell (1953). Recently Gill (1975) and DeWitt and Leetma (1977) derived equations that permit calculation of the Ekman pumping velocity at the equator from a known wind stress. The model by Gill (1975) was adopted for this study. It uses a frictional force which is proportional to velocity (Wyrtki, 1956). The solution is

$$(12) \qquad W = -\frac{(z+H)}{H} \cdot \frac{\beta(r^2 - \beta^2 y^2)\tau^x + 2r\beta^2 y\tau^y}{(r^2 + \beta^2 y^2)}$$

where z is the vertical coordinate positive upward, the origin is at the sea surface, H is the thickness of the wind driven layer, and r is the constant of proportionality between frictional force per unit mass and velocity. The other symbols were defined in Chapter III. The value of r was determined from the observations of Taft and Jones (1973), who calculated a vertical velocity of $8 \cdot 10^{-3}$ cm $s^{-1}$ at 28 m depth from carefully measured horizontal currents. The wind stress was .32 dynes/cm$^2$ at the time, and the depth of the core of the undercurrent was 100 m, which was assumed to be an appropriate value for H. The value of r calculated from (12) with y and $\tau^y$ equal to zero is $3 \cdot 10^{-6}$ $s^{-1}$. The Ekman pumping velocity was calculated in the equatorial Pacific from (12) using this value of r, z equal to H/2 and the observed monthly wind stress. These values were used to complete Fig. 16 near the equator and to carry out the calculations described in Chapter IV.

The geostrophic divergence was estimated at 2°N and 2°S by calculating the zonal gradient of the zonal geostrophic current. This estimate gives the correct sign of the horizontal divergence when the oceanic motions are composed of equatorial Rossby waves (Matsuno, 1966, Figs. 4 and 5) and is exactly the horizontal divergence when the oceanic motions are composed of equatorial Kelvin waves. The values at the equator were assumed equal to half the average of values calculated at 2°N and 2°S. The factor of one-half was introduced because observed displacements of the thermocline have maximum amplitudes on either side of the equator except near the eastern boundary (Fig. 4). The values at 4°N and 4°S were calculated as described in Chapter IV.

The sum of displacements calculated from the Ekman pumping velocity and the geostrophic divergence are in phase with observed displacements only in the region near the eastern boundary (Fig. 24), and not along the remainder of the equator. The vertical velocity calculated from the wind stress with (12) is very large along the equator; however, isotherms are not directly advected by this current because mixing is very intense. The response of the equatorial Pacific Ocean to annual forcing by the equatorial easterlies will be described in detail in a separate paper.

# VII. CONCLUSION

Annual variation in the depth of the thermocline has been described throughout the tropical Pacific Ocean and related to forcing by the trade winds. A large response in the ocean was found in the region from 4°N to 15°N. Near 6°N the monthly anomalies propagate westward at nearly the phase speed of non-dispersive Rossby waves. Near 10°N the monthly anomalies have the same phase across the ocean from the American coast to 145°E. A simple model of large-scale, low frequency currents is able to account for the observed variations in the thermocline. The model is driven by divergence in the Ekman layer set up by the surface wind stress, called Ekman pumping by Veronis (1973). It also incorporates the effect of planetary, geostrophic divergence inherent on a rotating sphere (Stommel, 1957). The oceanic response at 10°N is in phase with the Ekman pumping velocity, and the effect of geostrophic divergence is small. The response takes this form apparently because the forcing is strong and nearly zonally uniform. Geostrophic divergence is not negligible at 6°N, because the oceanic response is in the form of a westward propagating wave. The wave is formed apparently because the zonal length scale of the forcing function is nearly equal to the wave length of a free non-dispersive Rossby wave with a period of 1 year.

# LITERATURE CITED

Austin, T. S. 1957. Summary, Oceanographic and fishery data, Marquesas Islands Area, August-September, 1956 (EQUAPAC). U.S. Fish. and Wild. Serv. Spec. Sci. Rep., No. 217, 186 pp.

Bryden, H. L. 1977. Geostrophic comparisons from moored measurements of current and temperature during the Mid-Ocean Dynamics Experiment. Deep Sea Res., 22, 667-681.

Cromwell, T. 1953. Circulation in a meridional plane in the central equatorial Pacific. J. Mar. Res., 12, 196-213.

DeWitt, P. W. and A. Leetma. 1978. A simple Ekman-type model for predicting thermocline displacement in the tropical Pacific. J. Phys. Oceanogr., in review.

Ekman, V. W. 1905. On the influence of the earth's rotation on ocean-currents. Ark. mat. astron. o. fys. Bd. 2: No. 11, 1-52.

Fedorov, K. N. 1961. Seasonal variations of equatorial currents in the ocean. Problems in Dynamical Oceanography, A. I. Fel'zenbaum, Ed., 156-160, (Trans. I. Shlechtman, Israel Program for Scientific Translations, 1968).

Gill, A. E. 1975. Models of equatorial currents. _Proc. Symp. Num. Models of Ocean Circ._, Durham, N. H., 1972, U.S. Nat. Acad. Sci., 181-203.

Gill, A. E. and P. P. Niiler. 1973. The theory of the seasonal variability in the ocean. _Deep Sea Res._, 20, 141-177.

Greenspan, H. P. and L. N. Howard. 1963. On a time-dependent motion of a rotating fluid. _J. Fluid Mech._, 17, 384-404.

Hayes, J. G. 1970. Curve fitting by polynomials in one variable. _Numerical Approximation to Functions and Data_, J. G. Hayes, Ed., The Athlene Press, Univ. of London, London, 43-64.

Hurlburt, H. E., J. C. Kindle and J. J. O'Brien. 1976. A numerical simulation of the onset of El Nino. _J. Phys. Oceanogr._, 6, 621-631.

King, J. E. and M. S. Doty. 1957. Preliminary report on expedition Eastropic. _U.S. Fish and Wild. Serv. Spec. Sci. Rep._, No. 201, 155 pp.

Knauss, J. A. 1962. Equatorial current systems. _The Sea_, Vol. 2, M. N. Hill, Ed., Interscience Publishers, New York, 235-252.

Lighthill, M. J. 1969. Dynamic response of the Indian Ocean to onset of the southwest monsoon. _Phil. Trans. Roy. Soc. London_, A, 265, 45-92.

Love, C. M., Ed. 1971. Eastropac Atlas 3. 1972a. Eastropac Atlas 1. 1972b. Eastropac Atlas 5. 1973. Eastropac Atlas 7. 1975. Eastropac Atlas 9. Circ. 330, Nat. Mar. Fish. Serv., Washington, D. C.

Matsumo, T. 1966. Quasi-geostrophic motions in the equatorial area. J. Met. Soc. Japan., 44, 25-43.

McCreary, J. P. 1976. Eastern tropical ocean response to changing wind systems: with application to El Nino. J. Phys. Oceanogr., 6, 632-645.

McCreary, J. P. 1977. Eastern ocean response to changing wind systems. Ph.D. dissertation, Univ. of Calif., San Diego.

Meyers, G. 1974. The effect of wind stress on transport of the Pacific North equatorial current. M. S. thesis, Univ. of Hawaii.

Meyers, G. 1975. Seasonal variation in transport of the Pacific North Equatorial Current relative to the wind field. J. Phys. Oceanogr., 5, 442-449.

Meyers, G. 1976. Sverdrup transports and Ekman divergences in the tropical Pacific Ocean. Unpublished MS. Read at AGU Spring Meeting, Washington, D. C.

Phillips, N. A. 1963. Geostrophic motion. Rev. of Geophys., 1, 123-176.

Reid, J. L. 1965. Intermediate waters of the Pacific Ocean. Johns Hopk. Oceanogr. Stud., No. 2, 85 pp.

Reid, J. L., R. S. Arthur and E. B. Bennet, Eds. 1965. Oceanic observations of the Pacific: 1957. Berkley and Los Angeles, Univ. of Calif. Press.

Robinson, M. K. 1976. Atlas of North Pacific Ocean monthly mean temperatures and mean salinities of the surface layer. Naval Oceanogr. Office Ref. Publ. 2, Dept. of the Navy, Washington, D. C., 14 pp., 173 figs.

Sader, J. C. 1976. Comments on "Low-level flows over the GATE area during summer 1972". Mon. Weath. Rev., 104, 650-652.

Seckel, G. R., 1968. A time-sequence of oceanographic investigation in the North Pacific trade wind zone. Trans. Am. Geophys. Un., 49, 377-387.

Stommel, H. 1957. A survey of ocean current theory. Deep Sea Res., 4, 149-184.

Taft, B. A. and J. Jones. 1973. Measurements of the equatorial undercurrent in the eastern Pacific Ocean. Progress in Oceanogr., 6, B. Warren, Ed., Pergamon Press, Oxford, 47-110.

Veronis, G. 1973. Large scale ocean circulation. Adv. Appl. Mech., 13, 1-92.

Veronis, G. and H. Stommel. 1956. The action of variable wind stresses on a stratified ocean. J. Mar. Res. 15, 43-75.

Wert, R. T. 1976. The oceanic bathythermograph data set. Fleet Numerical Weather Central, Monterey, Ca. Purchase Request no. 63134-5132-2525, 61 pp.

White, W. B. 1977. Annual forcing of baroclinic Rossby waves in the tropical North Pacific Ocean. J. Phys. Oceanogr., 7, 50-61.

White, W. B. 1977. The wind-driven seasonal cycle of the main thermocline in the mid-latitude North Pacific. J. Phys. Oceanogr., in review.

White, W. and R. Wylie. 1977. Annual and seasonal maps of the residual temperature in the upper waters of the western north Pacific from 1954-1974. SIO Ref. #77-28, Scripps Inst. of Oceanogr., Univ. of Calif., San Diego.

Wyrtki, K. 1956. The computation of oceanic and meteorological fields of motion with friction proportional to the velocity. Mar. Res. Indonesia, 2, 1-26.

Wyrtki, K. 1964. The thermal structure of the eastern Pacific Ocean. Deut. Hydrogr. Zeit. Erg. R. A, no. 6, 1-84.

Wyrtki, K. 1974. Sea level and the seasonal fluctuations of the equatorial currents in the Western Pacific Ocean. J. Phys. Oceanogr., 4, 91-103.

Wyrtki, K. and G. Meyers. 1975. The trade wind field over the Pacific Ocean. Part I. The mean field and the mean annual variation. Hawaii Inst. Geophys. Rep. no. HIG-75-1, 26 pp., 25 figs.

Wyrtki, K. and G. Meyers. 1975. The trade wind field over the Pacific Ocean. Part II. Bimonthly fields of wind stress 1950-1972. Hawaii Inst. Geophys. Rep. no. HIG-75-2, 16 pp., 138 figs.

Wyrtki, K. and G. Meyers. 1976. The trade wind field over the Pacific Ocean. J. Appl. Met., 15, 698-704.

Wyrtki, K., Meyers, G., McLain, D. and W. Patzert. 1977. Variability of the thermal structure in the central equatorial Pacific Ocean. Hawaii Inst. Geophys. Rep. HIG-77-1, 32 pp., 43 figs.

Yoshida, K. 1955. An example of variations in oceanic circulation in response to the variations in the wind field. J. Oceanogr. Soc. Japan, 11, 103-108.

Yoshida, K. and H. L. Mao. 1957. A theory of upwelling of large horizontal extent. J. Mar. Res., 16, 40-57.